LBL-8271
Revised
UC-70

MASTER

A STUDY OF REGIONAL TEMPERATURE AND THERMOHYDROLOGICAL EFFECTS OF AN UNDERGROUND REPOSITORY FOR NUCLEAR WASTES IN HARD ROCK

J. S. Y. Wang, C. F. Tsang,
N. G. W. Cook and P. A. Witherspoon

October 1979

Prepared for the U. S. Department of Energy
under Contract W-7405-ENG-48

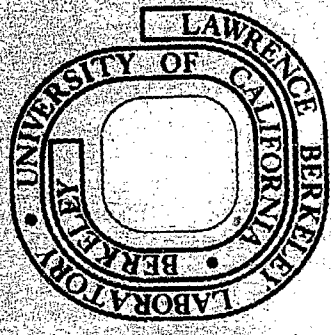

An abbreviated version of this report was submitted for publication in June 1979 to the Journal of Geophysical Research

LBL-8271
Revised

A STUDY OF REGIONAL TEMPERATURE AND THERMOHYDROLOGICAL EFFECTS OF AN UNDERGROUND REPOSITORY FOR NUCLEAR WASTES IN HARD ROCK

J. S. Y. Wang, C. F. Tsang, N. G. W. Cook and P. A. Witherspoon

Earth Sciences Division
Lawrence Berkeley Laboratory
University of Califo·-ia
Berkeley, California 94720

October 1979

Funding for this work was supplied by the U. S. Department of Energy under contract number W-7405-ENG-48.

ABSTRACT

Heat released by the radioactive decay of nuclear wastes in an underground repository causes a long-term thermal disturbance in the surrounding rock mass. The nature of this disturbance for a planar repository 3000 m in diameter at a depth of 500 m below surface is investigated for various waste forms. The effects of changes in the density and viscosity of groundwater caused by the temperature changes on the flow through a simple model of a vertical fracture connected to a horizontal fracture in a rock mass are evaluated. It is concluded that different waste forms and time periods before burial have significant effects on the thermal disturbance and that buoyant groundwater flow is a function of both the vertical and horizontal fracture transmissivities, as well as the changes in temperature. Loaded initially with a power density of 10 W/m^2 of spent fuel assemblies 10 years after discharge from a reactor, the maximum increase in temperature of the repository in granite is about 50°C and the epicentral thermal gradient about 70°C/km.

TABLE OF CONTENTS

LIST OF FIGURES

LIST OF TABLES

NOMENCLATURE

b	fracture aperture	(L)
C	specific heat	$(L^2t^{-2}T^{-1})$
D	depth of repository	(L)
g	gravity acceleration	(Lt^{-2})
h	head	(L)
I_o	zeroth order modified Bessel function of the first kind	
k	permeability	(L^2)
K	thermal conductivity	$(MLt^{-3}T^{-1})$
L	distance from the center of repository to the recharge and discharge zone	(L)
M	mass per unit width	(ML^{-1})
P	pressure	$(ML^{-1}t^{-2})$
$\vec{q}$	mass flux	$(ML^{-2}t^{-1})$
R	radius of disk-shaped repository	(L)
r, r'	radial coordinate from the repository axis	(L)
T	temperature	(T)
t, t'	time	(t)
Δt	transit time	(t)
V	source function	(L^{-1})
$\vec{v}$	flux velocity	(Lt^{-1})
Z	vertical displacement of water level initially at repository depth	(L)
z	vertical coordinate from the ground surface	(L)
β	compressibility of water	$(M^{-1}Lt^2)$
κ	diffusivity	(L^2t^{-1})
ρ	density	(ML^{-3})
ψ	power density	(Mt^{-3})
μ	dynamic viscosity	$(ML^{-1}t^{-1})$
ν	kinematic viscosity	(L^2t^{-1})

Superscripts and subscripts

o	ambient
b	buoyancy
dc	discharge zone
p	pressure
R	rock
rc	recharge zone
T	temperature
x	horizontal
w	waste
z	vertical
-	effective head

INTRODUCTION

Significant quantities of nuclear wastes exist already and continue to be produced (Department of Energy, 1978). At present, most of these wastes are stored in near-surface facilities. Although every precaution is taken to protect man and the environment from the potential hazard posed by these wastes, near-surface storage is not regarded as a satisfactory long-term proposition. Disposal of nuclear wastes by deep burial in suitable geologic formations is generally favored (Interagency Review Group, 1978). The principal attraction of disposal by deep burial is that it provides a high degree of physical isolation of the nuclear waste from the biosphere. The principal concern of deep burial is that at no stage should toxic components of these wastes find their way back to the biosphere at levels which are not completely harmless.

A wealth of scientific knowledge and engineering experience exists concerning the excavation of underground openings in a wide variety of geologic media. Unfortunately no comparable experience exists concerning the effects of the generation of heat within such openings nor of the leakage of materials from such openings back to the biosphere.

Salt formations have generally been preferred as candidates for deep geological disposal for a number of reasons (National Research Council, 1957). The relatively high thermal conduction of salt facilitates the dissipation of heat released by the radioactive decay of nuclear wastes. The viscous plasticity of salt, particularly at elevated temperatures, assures that the excavation

within which the wastes are disposed will, in the long term, seal themselves by deformation of the salt itself, and the presence of the salt attests to very slow dissolution and transport by movement of groundwater.

However, other geological media may be equally or even better suited for construction of deep underground repositories for nuclear wastes, provided the openings and access ways to the repository can be sealed adequately. The permeability of intact pieces of many crystalline and argillaceous rocks is at least as low as that of salt. However, the permeability of masses of such rocks arises mainly from the hydraulic conductivity of joints and fractures pervading them, but may still be sufficiently small to retard the movement of groundwater between the repository and the biosphere to an adequate degree.

The purpose of this paper is to study three important aspects concerning the design and performance of such underground repositories for the disposal of nuclear wastes in hard rock. First, the heat released by the radioactive decay of the nuclear wastes causes changes in the spatial and temporal distributions of temperature in the rock mass within which the repository is located. These changes in temperature produce thermally induced components of compressive stress in the heated portions of this rock mass and tensile components of stress outside of this zone. These thermally induced changes in stress may affect the performance and design of a repository. An understanding of the distribution of temperatures around a repository is necessary to evaluate the thermally induced changes in stress. However, the evaluation of the stress changes is not part of this paper. Second, the magnitude and temporal changes of the temperatures in the rock mass surrounding the repository are affected

by the type of waste and the time after its removal from the reactor. The effects of different wastes on the temporal changes in temperature are examined. Finally, changes in the temperature of the groundwater in the rock mass containing the repository affect both the density and viscosity of the water significantly. These changes in density and viscosity may result in perturbations of the original hydrological flow, which could affect the performance of the repository in isolating toxic components of the wastes from the biosphere. A model of buoyant groundwater flow through a simple fracture system is used to assess the magnitude of this phenomenon.

TEMPERATURE FIELD

Repository Model

To study the long-term regional changes in temperature in the rock mass the repository is idealized to be a flat circular disk loaded uniformly with nuclear waste at time t = 0. The repository is assumed to be a depth, D, of 500 m below the surface in granite and to have a radius, R, of 1500 m. The principal mode of heat transfer from the nuclear waste to the rock mass is assumed to be by linear heat conduction. This has been proved to be a good assumption based on recent Stripa data analysis (Hood, 1979).

The temperature field, T(r,z,t), resulting from heat conduction in the rock mass as a function of space and time is given by a solution to the diffusion equation:

$$\frac{1}{r}\frac{\partial}{\partial r}\left(r\frac{\partial T}{\partial r}\right) + \frac{\partial^2 T}{\partial z^2} = \frac{1}{\kappa_T}\frac{\partial T}{\partial t} \qquad (1)$$

$$\kappa_T = \frac{K}{\rho_R C_R}$$

where

r = the radial coordinate;

z = the axial depth below surface;

t = the time after loading;

κ_T = the thermal diffusivity;

K = the thermal conductivity;

ρ_R = the density of the rock; and

C_R = the specific heat of the rock.

Values for the thermal properties of granite and other hard rocks are given in Table 1.

Table 1: Thermal Properties of Rocks

Rock	K (W/m/°C)	ρ_R (kg/m^3)	C_R (J/kg/°C)	κ_T (10^{-6}m^2/sec)
Granite [a]	2.5	2600	836	1.15
Stripa granite [b]	3.2	2600	837.36	1.47
Basalt [c]	1.62	2865	1164	0.486
Shale [d]	0.90	2300	1000	0.391

a Kappelmeyer and Haenel, 1974

b Pratt et al., 1977

c Martinez-Baez and Amick, 1978

d Fairchild et al., 1976

By integrating the solution for an instantaneous point source of heat over the radius of the repository, R, in the plane z = -D (Carslaw and Jaeger, 1959), the unit of strength of an instantaneous disk heat source can be found.

$$V_{-D}(r, z, t) = \frac{1}{4(\pi\kappa_T t^3)^{1/2}} \int_0^R \exp\left[-\frac{r^2 + r'^2 + (z + D)^2}{4\kappa_T t}\right] I_o\left(\frac{rr'}{2\kappa_T t}\right) r'dr', \quad (2)$$

where I_o is the zeroth order modified Bessel function of the first kind. On the axis of the disk (r = 0), V_{-D} is simply

$$V_{-D}(0, z, t) = \frac{1}{2(\pi\kappa_T t)^{1/2}} \left\{ \exp\left[-\frac{(z + D)^2}{4\kappa_T t}\right] - \exp\left[-\frac{R^2 + (z + D)^2}{4\kappa_T t}\right] \right\}$$

which depends only on the distances from the point on the axis to the center and to the perimeter of the disk. If the radius R is much larger than the distance $|z + D|$, $V_{-D}(0, z, t)$ is reduced to the instantaneous plane heat source with heat conduction in the z-direction.

When heat is released from the nuclear waste at an average rate $\phi(t')$ by the disk-like repository from time t' = 0 to time t' = t, the temperature change at any point (r, z) is:

$$\Delta T(r, z, t) = \frac{1}{\rho_R C_R} \int_0^t \phi(t') V_{-D}(r,z,t - t')dt' - \frac{1}{\rho_R C_R} \int_0^t \phi(t') V_{+D}(r,z,t - t')dt' \quad (3)$$

The first term in this equation represents the change in temperature from the disk-like source in the infinite medium and the second term is a correction (by the method of image) for the presence of a boundary at constant temperature at the ground surface, z = 0.

For the purposes of this paper, equations (2) and (3) have been integrated numerically for a number of expressions $\psi(t')$.

Temperatures on the z-axis for simple functions $\psi(t')$, such as constant power, exponential decay of power (Hodgkinson and Bourke, 1978), and a decrease in power inverse to the square root of time can be expressed in terms of tabulated functions. These are given in Table 2 and can be used to check the accuracy of the numerical solutions to equations (2) and (3). In this paper, numerical results reproduce these analytical solutions to within 0.01°C.

Table 2: Analytic solutions of temperature rise on the z-axis of disk source.

Power form	Power density $\psi(t)$	Solution form* $f(x, t)$
Constant	$\psi(0)$	$\frac{\psi(0)(\kappa_T t)^{1/2}}{K}\,\mathrm{ierfc}(x)$
Exponential decay	$\psi(0)\exp(-\lambda t)$	$\frac{\psi(0)}{K}(\kappa_T/\lambda)^{1/2}\,\mathrm{imW}[(\lambda t)^{1/2} + ix]$
Inverse square root	$2T_0K/(\pi\kappa_T t)^{1/2}$	$T_0\,\mathrm{erfc}(x)$

* $\Delta T(0, z, t) = f\{[(z + D)^2/4\kappa_T t]^{1/2}, t\} - f\{[(R^2 + (z + D)^2)/4\kappa_T t]^{1/2}, t\}$

$- f\{[(z - D)^2/4\kappa_T t]^{1/2}, t\} + f\{[(R^2 + (z - D)^2)/4\kappa_T t]^{1/2}, t\}$

ierfc = first integral of complementary error function

erfc = complementary error function

imW = imaginary part of the error function of complex argument.

Different Forms of Waste

At present, consideration is being given to the disposal of two principal forms of nuclear waste, both generally known as high-level waste. They are: spent fuel as discharged from a reactor; and the products from reprocessing spent fuel to recover the uranium and plutonium. Assuming that either form of high-level waste is buried 10 years after discharge from the reactor, at an initial loading density in the repository of 10 W/m^2, the power densities of the two principal waste forms in the plane of the repository and of their main constituents as a function of time are as illustrated in Figure 1 (Kisner et al., 1978). The nuclear wastes contain fission products and actinides (U, Pu, ...). The fission products generate most of the heat in the early life of the wastes but decay very rapidly, with an approximate half-life of 30 years. The actinides and their daughter nuclei are the main heat source later on. With reprocessing treatment to remove most of the actinides (99.5%), the power density of reprocessed waste is much smaller after a long time than that of spent fuel.

The curves in Figure 1 give numerically the $\varphi(t')$ used in equation (3). They were used to calculate the temperature changes in the rock mass containing the repository as described above. Examples of these changes in temperature and isotherms for a repository containing spent fuel or reprocessed waste 10, 100, 1000 and 10,000 years after burial in the repository are as illustrated in Figures 2 through 5. The temperature profiles along the vertical axis through the center of the repository and along the radial axis in the plane of the repository are also shown in these figures. At early times of 10 and 100

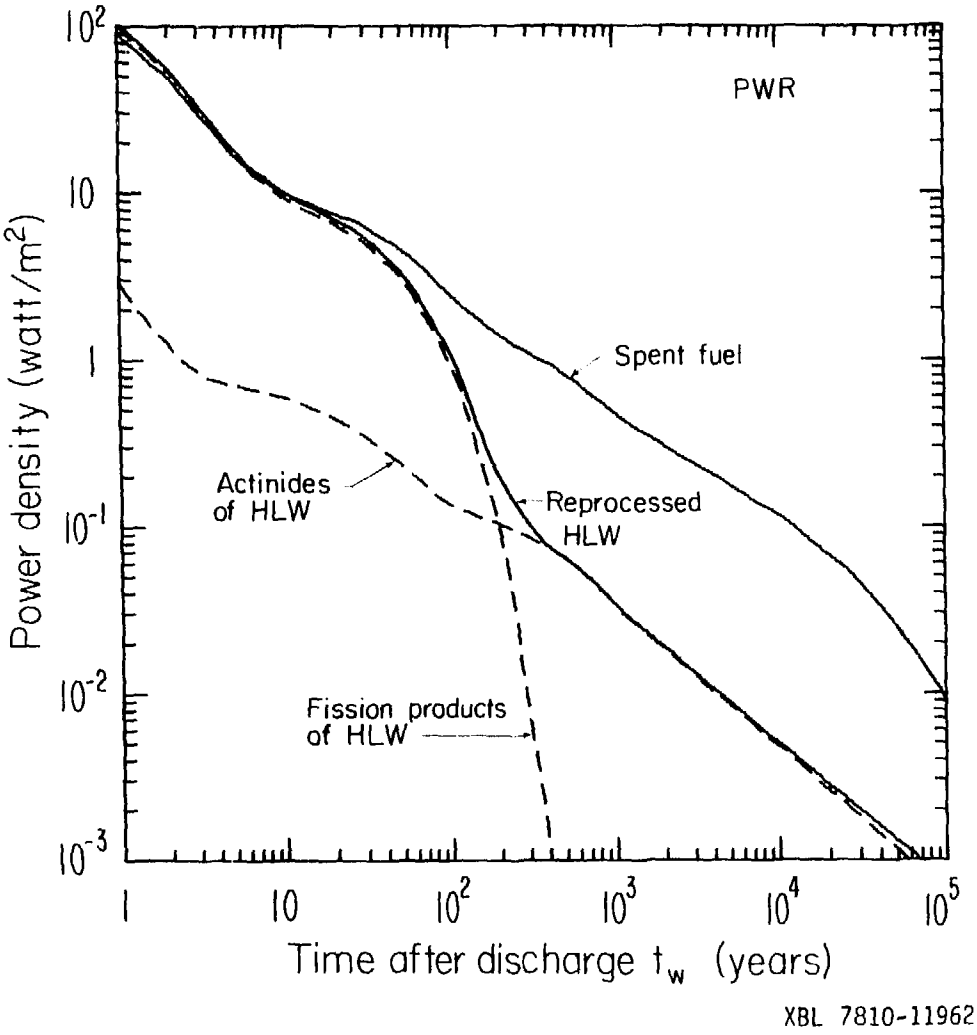

Figure 1. Areal power density of heat generated by the stored nuclear wastes.

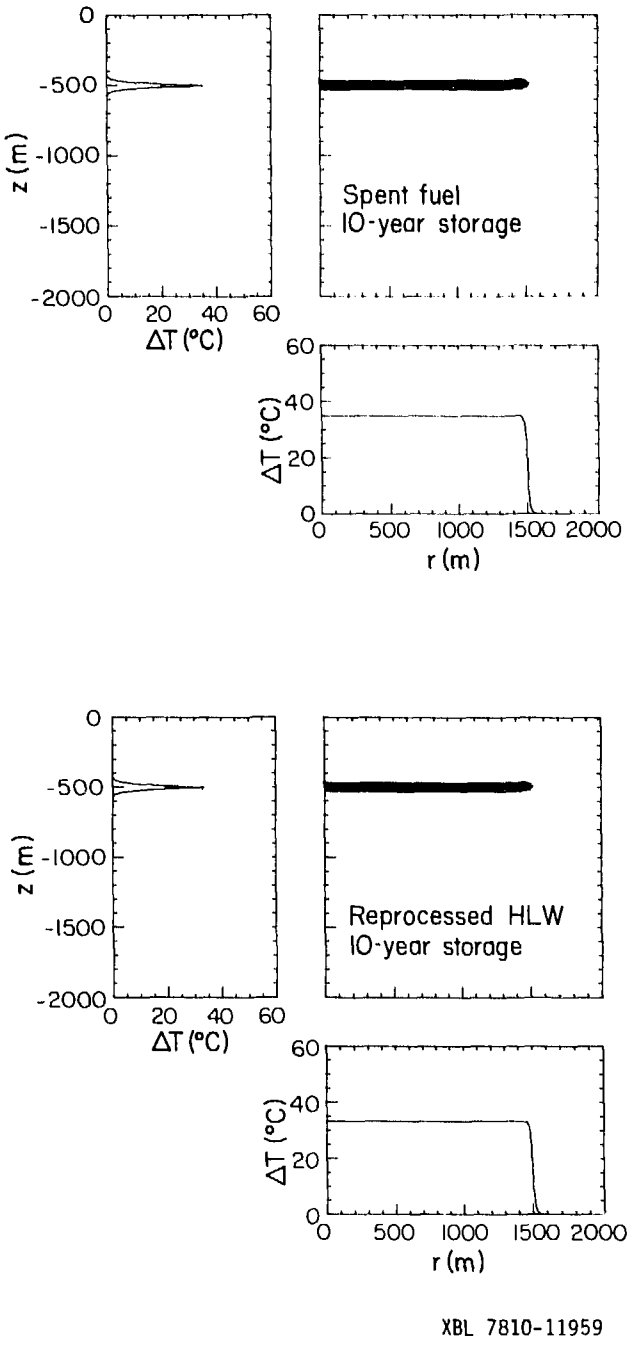

Figure 2. Isotherms and profiles of temperature rise around repository after 10 years of waste storage.

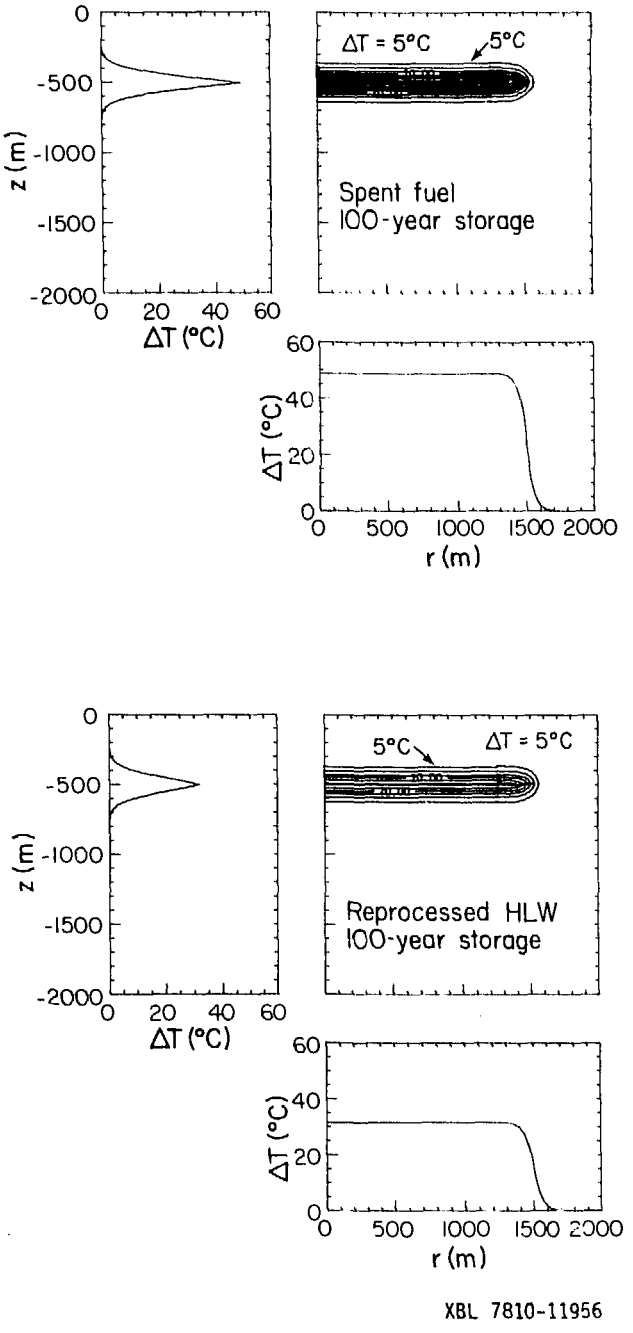

Figure 3. Isotherms and profiles of temperature rise around repository after 100 years of waste storage.

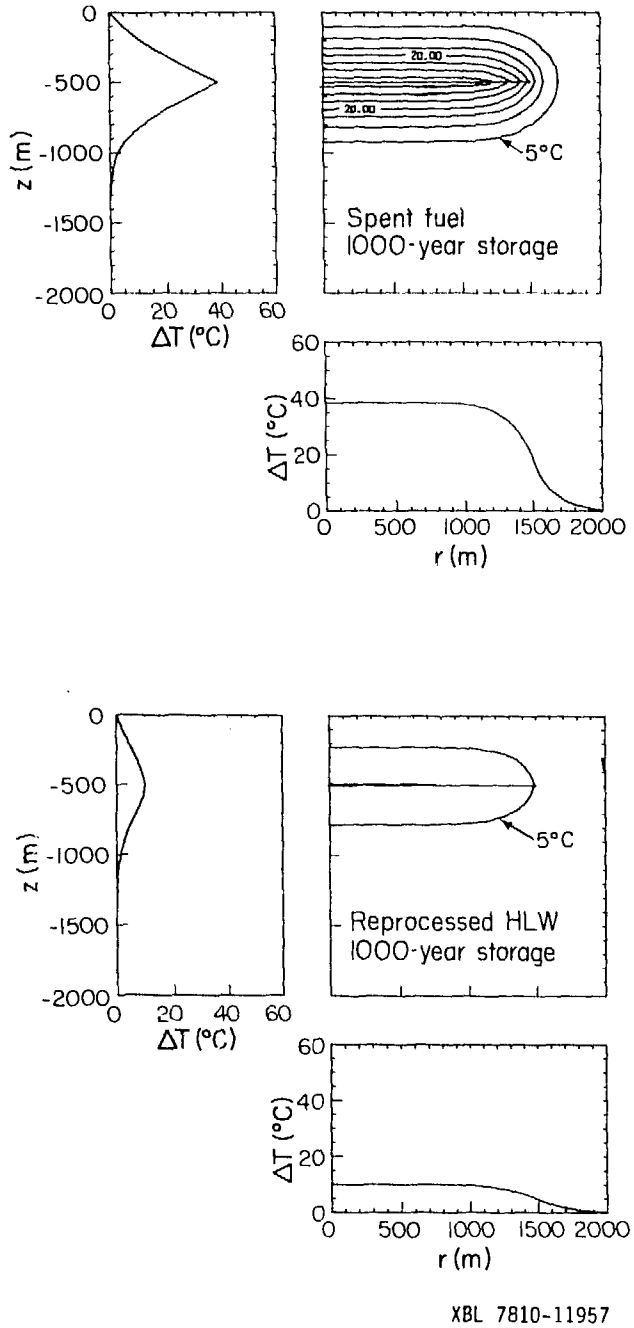

Figure 4. Isotherms and profiles of temperature rise around repository after 1000 years of waste storage.

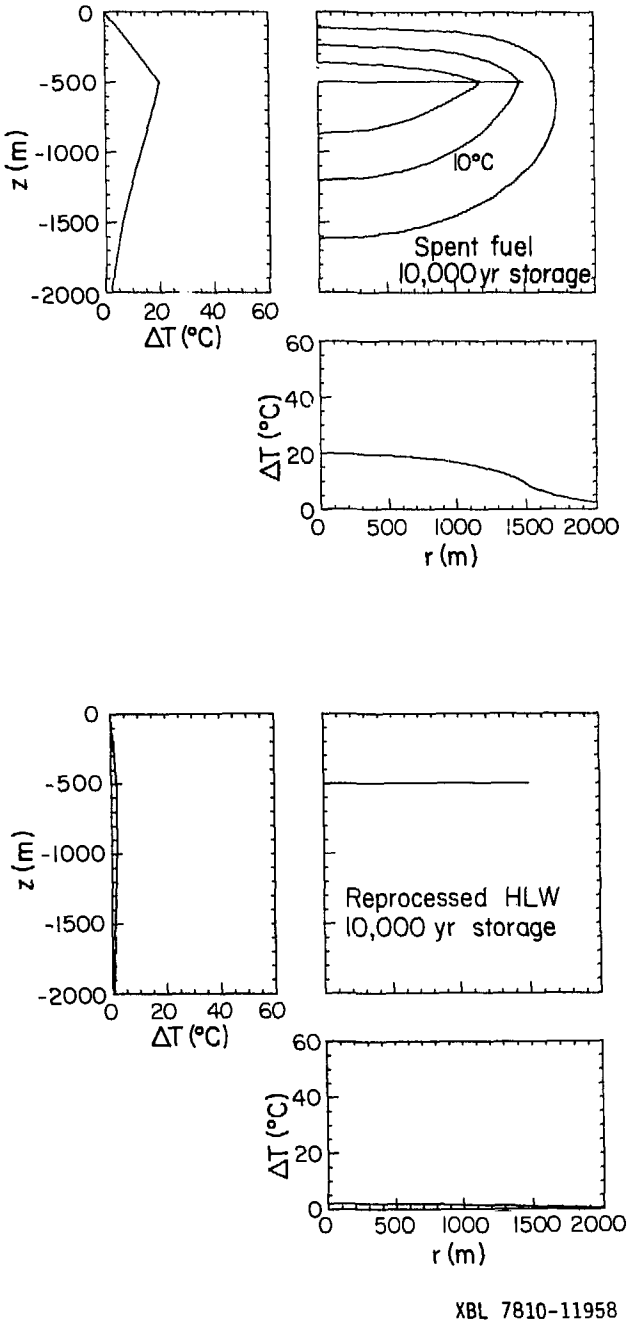

Figure 5. Isotherms and profiles of temperature rise around repository after 10,000 years of waste storage.

years, temperature changes and large temperature gradients are induced only in the vicinity of the repository. Most of the heat is conducted vertically upward and downward from the repository. The extent of heat diffusion is approximately $4\sqrt{\kappa_T t}$. Only later on after 1000 years, when the heat flux from the repository leaks out at the ground surface, is an approximate linear temperature profile from the repository to the ground surface maintained.

It is important to note how much greater the magnitudes of the temperature changes for spent fuel are than for reprocessed waste, especially after 1000 years of burial. The power density of spent fuel is 10-fold greater than that of reprocessed waste after 1000 years.

The maximum average temperature in a repository arises at its center and is plotted as a function of time after burial in Figure 6. For both spent fuel and reprocessed waste this temperature reaches a maximum after a period of less than 100 years and thereafter decays very slowly (especially for spent fuel) over a period of many thousands of years. The maximum temperature and all other temperatures are of course proportional to the power density with which the repository is loaded.

To study the far-field effects and, in particular those at the surface, the maximum ground surface temperature grad ent at the epicenter above the repository has been calculated for both forms of waste and is as illustrated in Figure 7. This gradient and the corresponding heat flow $K\nabla T$ through the surface (in HFU = $\mu cal/cm^2/sec$) reach maximum values at about 2400 years after burial and 1300 years after burial for the spent fuel and reprocessed waste,

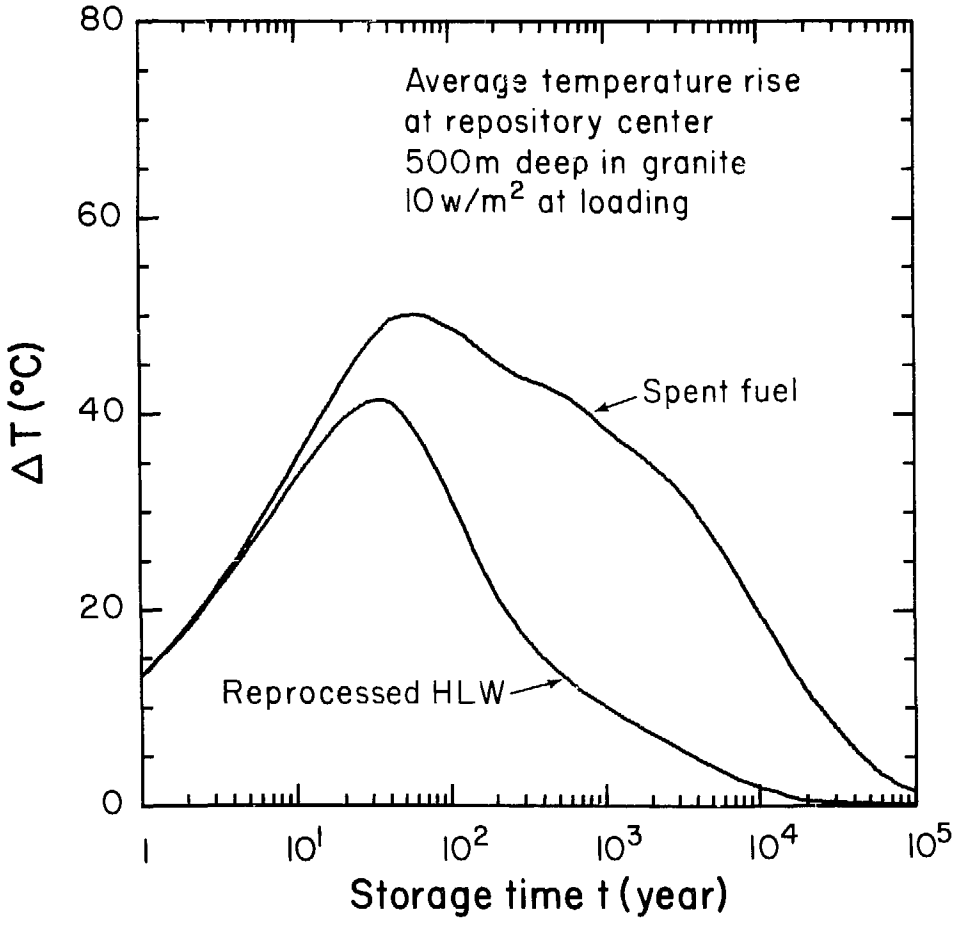

Figure 6. Temperature rise at the center of a disk-shaped repository in granite stored uniformly with nuclear wastes.

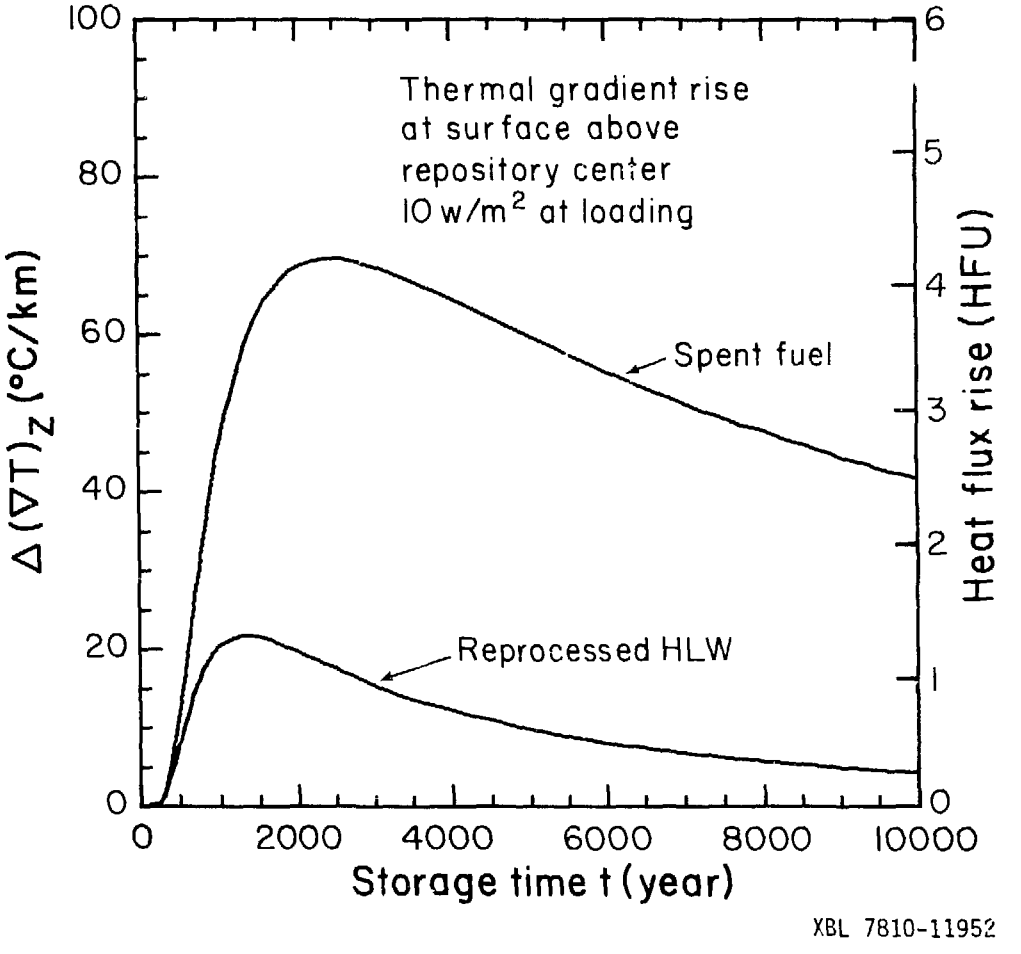

Figure 7. Ground surface epicentral thermal gradient rise above a disk-shaped nuclear waste repository with radius of 1500 m, and 500 m deep in granite.

respectively. The maximum value of the temperature gradient for the spent fuel, 70°C/km, is about three times greater than that of the reprocessed waste, 22°C/km. The total thermal gradient is of course the sum of the original geothermal gradient, typically of 30°C/km, and the thermal gradient induced by the repository.

The power output of various waste forms as a function of time, $\wp(t')$, in a log-log plot can be approximated by segments of straight lines over periods of time after discharge from the reactor, as shown in Figure 8. Values of the maximum changes in temperature at the center of the repository as a function of time, and of the epicentral thermal gradient have been calculated for functions of $\wp(t')$ in which power varies inversely as time after discharge from a reactor $t_w = t' + 10$ to the power $\varepsilon = 1$, 2/3 and 1/2, as well as for $\wp(t')$ representing the power output of spent fuel as illustrated in Figure 1. The results of these calculations are as shown in Figure 9. In Figure 10, similar results for reprocessed waste are shown together with those for inverse square root power in time of storage t' and for an exponential decay of power output with a half-life of 30 years. From this figure it can be seen that, because the output of the two principal forms of nuclear wastes decays with time faster than that corresponding to inverse square root, the maximum temperature in any repository must reach a peak value and then decays, such as that illustrated in Figure 6. The power function of inverse square root in time of storage represents a constant temperature plane heat source in an infinite medium. The onset of cooling after a thousand years is due to the interaction of the heat source with the ground surface boundary condition.

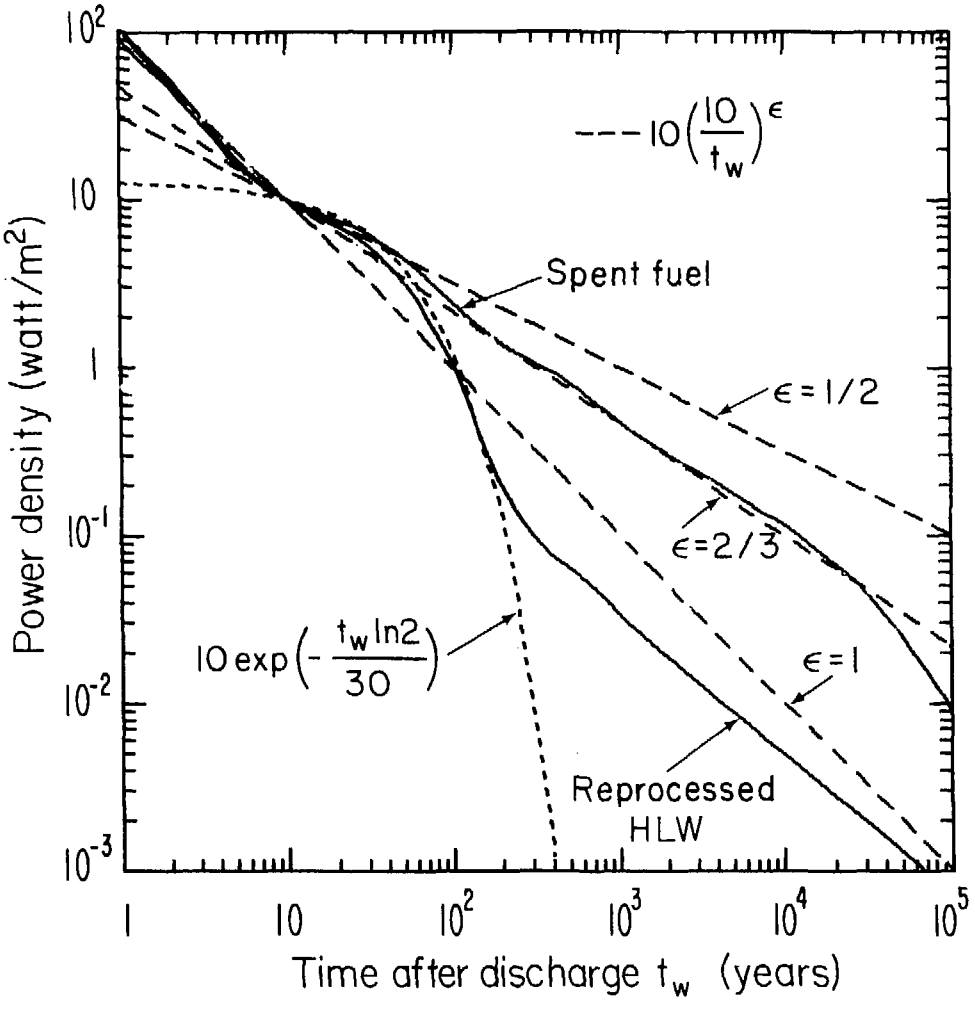

Figure 8. Comparison of power densities of nuclear waste with simple functions of inverse power laws and exponential decay of 30-year half life.

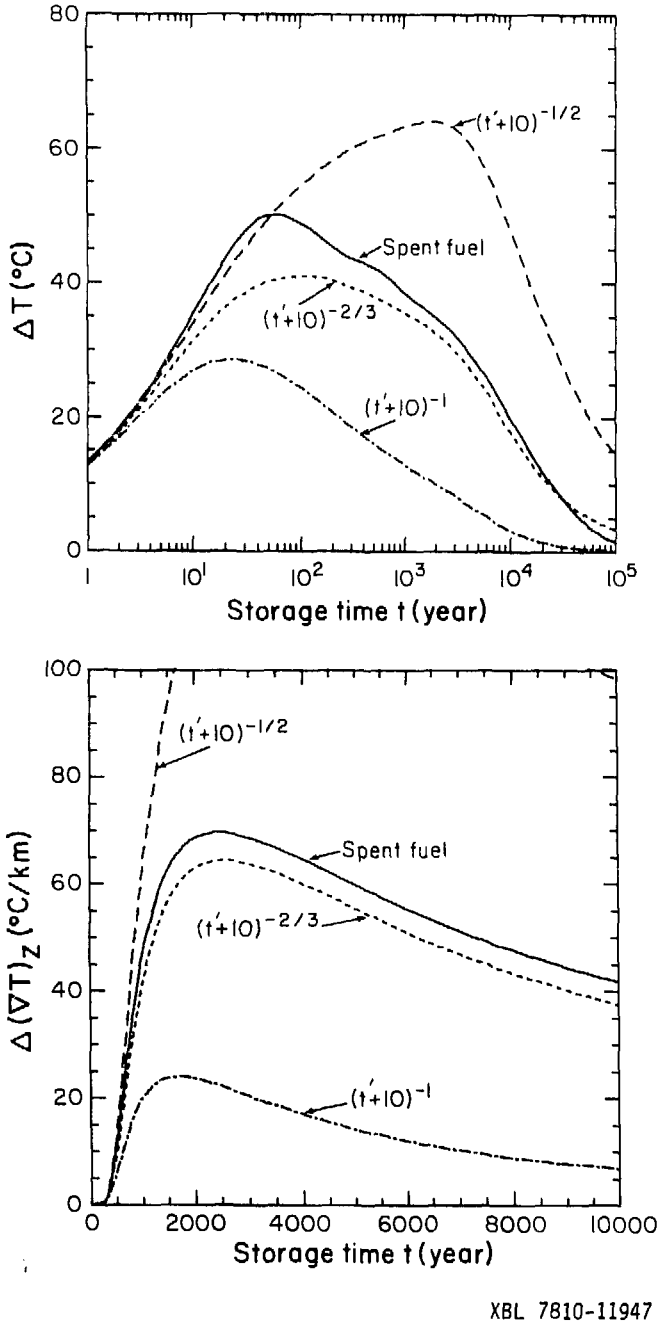

Figure 9. Comparison of repository temperature and ground surface thermal gradient of spent fuel with the results calculated with simple function of inverse power laws.

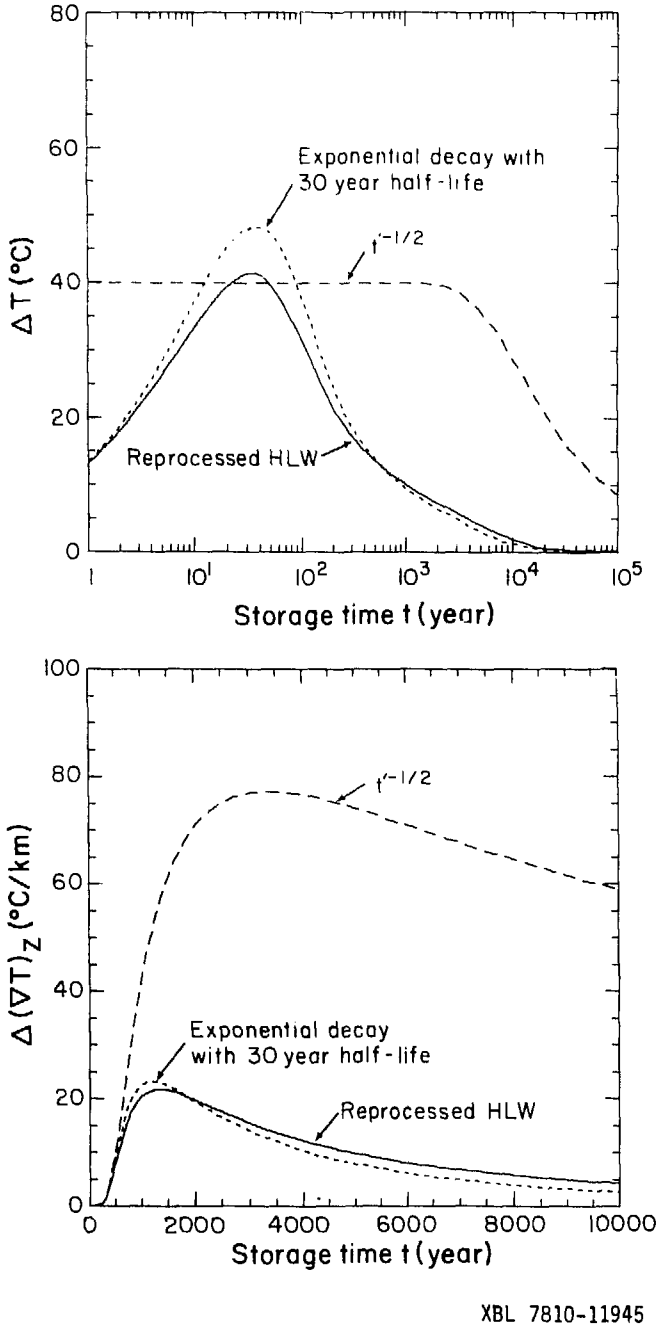

Figure 10. Comparison of repository temperature and ground surface thermal gradient of reprocessed waste with the results calculated with exponential function and inverse square root.

The decay in power output of nuclear wastes as a function of time is determined by their composition and age; different fuel cycles yield wastes with different compositions. The U and Pu recovered from the discharged fueld can be used in new fuel elements and recycled to the nuclear reactors. The fuel cycle can also be operated so that neither of these elements is recovered and recycled or either of them is recycled. The nonrecycled U or Pu can be stored together with the reprocessed waste or stored separately. Therefore, numerous waste types are available. Figures 11 and 12 are the power densities of different waste types originating from the same amount of fuel, 1 MTHM (MTHM = metric ton of heavy metal U), charged to a pressurized water reactor (PWR) and a boiling water reactor (BWR), respectively. To evaluate some of the effects of different fuel cycles, it has been assumed that the repository is loaded with 0.01 MTHM/m^2 which is equivalent to a total load in the repository of 0.71 x 10^6 MTHM. The repository temperatures and epicentral thermal gradients as a function of time for different wastes from PWR and BWR are illustrated in Figures 13 and 14. The maximum values of repository temperatures and epicentral thermal gradients are summarized in Table 3. It can be seen that the differences in temperature for the different fuel cycles for a repository loaded with 0.01 MTHM/m^2 arise mainly from the variations of initial power density.

In Table 3, results are also given for a repository loaded at an initial power density of 10 W/m^2. The loading power densities and the repository temperature and epicentral thermal gradient as a function of time are illustrated in Figures 15-18. Even at a constant power density 10 W/m^2, significant

differences among different waste types can be seen. The differences can be attributed to the amount of fission products at early times and the amount of Pu later on.

Table 3: Effects of Fuel Cycles

Nuclear reactor	Fuel-cycle	$(\Delta T)_{max}$ [a] °C [c]	$(\Delta(\nabla T)_z)_{max}$ [b] °C/km [c]	Power density at loading W/m^2 [c]	kW/canister
PWR	Spent fuel [d]	60 (50)	83 (70)	11.9 (10)	.548
	HLW+PuO_2:U-recycle [e]	65 (52)	86 (69)	12.5 (10)	2.61
	HLW:U+Pu recycle [f]	90 (40)	68 (30)	22.7 (10)	4.75
	HLW:U-recycle [g]	43 (42)	22 (22)	10.2 (10)	2.14
	HLW:no recycle [h]	43 (41)	22 (22)	10.3 (10)	2.16
BWR	Spent fuel [d]	50 (51)	73 (74)	9.96 (10)	.182
	HLW+PuO_2:U-recycle [e]	57 (54)	77 (73)	10.5 (10)	2.20
	HLW:U+Pu recycle [f]	71 (40)	59 (34)	17.5 (10)	3.65
	HLW:U-recycle [g]	35 (42)	19 (23)	8.30 (10)	1.74
	HLW:no recycle [h]	35 (42)	19 (23)	8.35 (10)	1.75

a $(\Delta T)_{max}$: maximum value of the average temperature rise at the center of the repository.

b $(\Delta(\nabla T)_z)_{max}$: maximum value of the ground surface thermal gradient rise at the epicenter above the repository.

c Values without parentheses correspond to 0.01 MTHM/m^2 waste capacity. Values with parentheses correspond to 10 W/m^2 power density.

d Fuel assembly discharge directly from the reactor.

e Reprocessed waste with U and Pu removed from the discharge fuel, U recycled in the reactor, and Pu stored together with the waste.

f Reprocessed waste with U and Pu removed from the discharge fuel and recycled in the mixed oxide reactor.

g Reprocessed waste with U and Pu removed from the discharge fuel and U recycled in the reactor.

h Reprocessed waste with U and Pu removed from the discharge fuel.

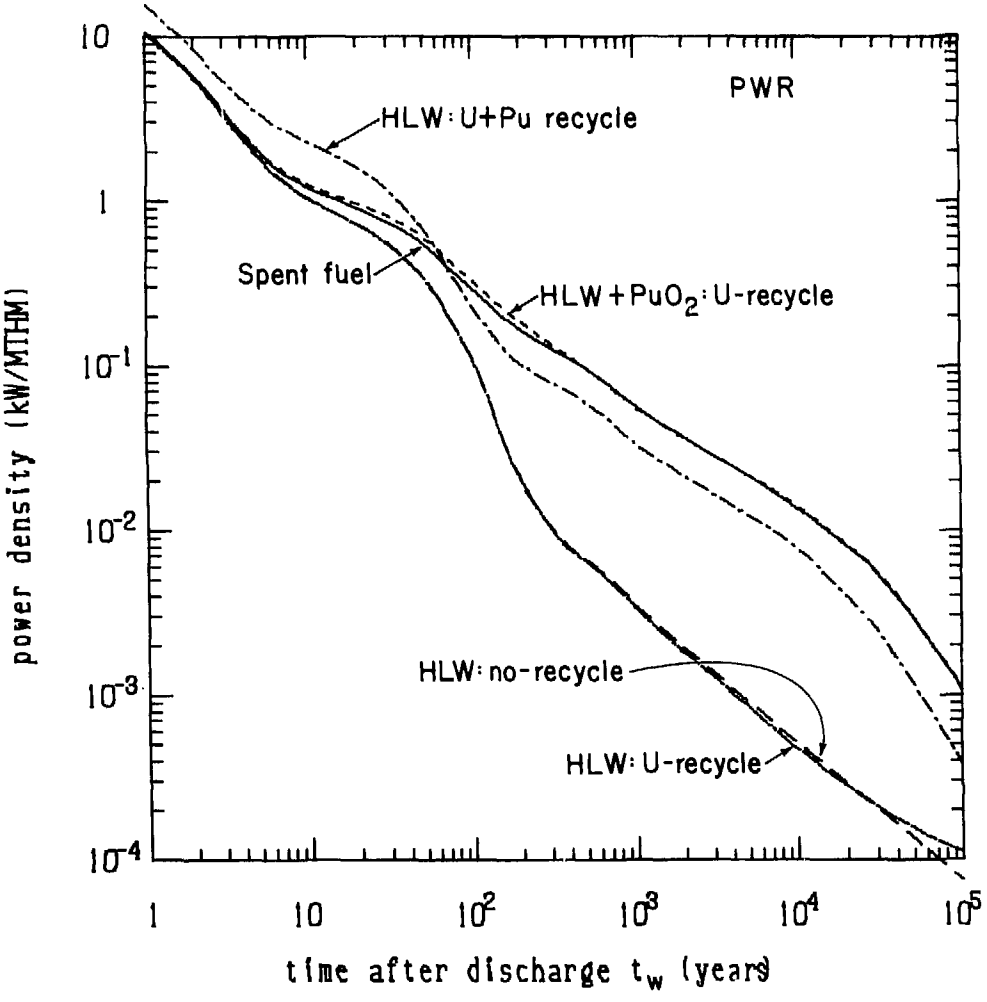

XBL 796-7551

Figure 11. Power densities of wastes from different fuel cycles originated from the same amount of fuel (1 MTHM) charged to a PWR.

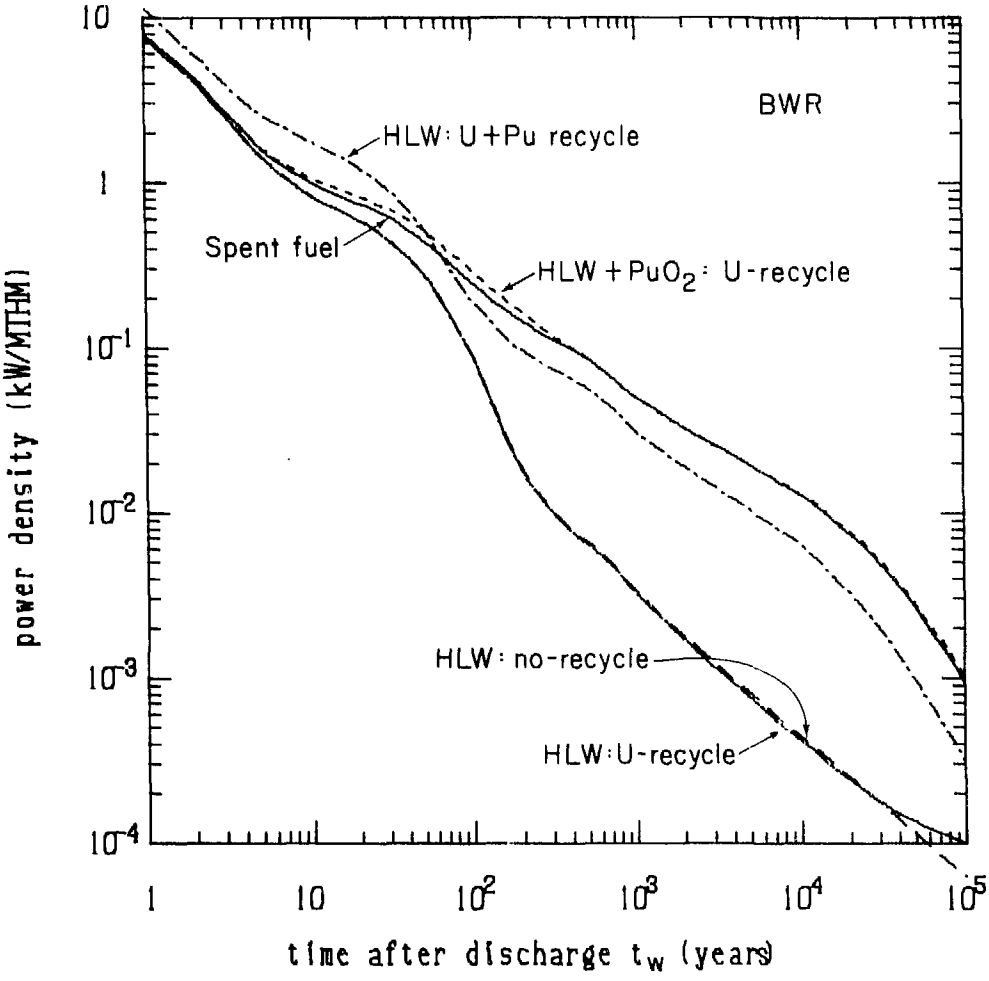

XBL 796-7550

Figure 12. Power densities of wastes from different fuel cycles originated from the same amount of fuel (1 MTHM) charged to a BWR.

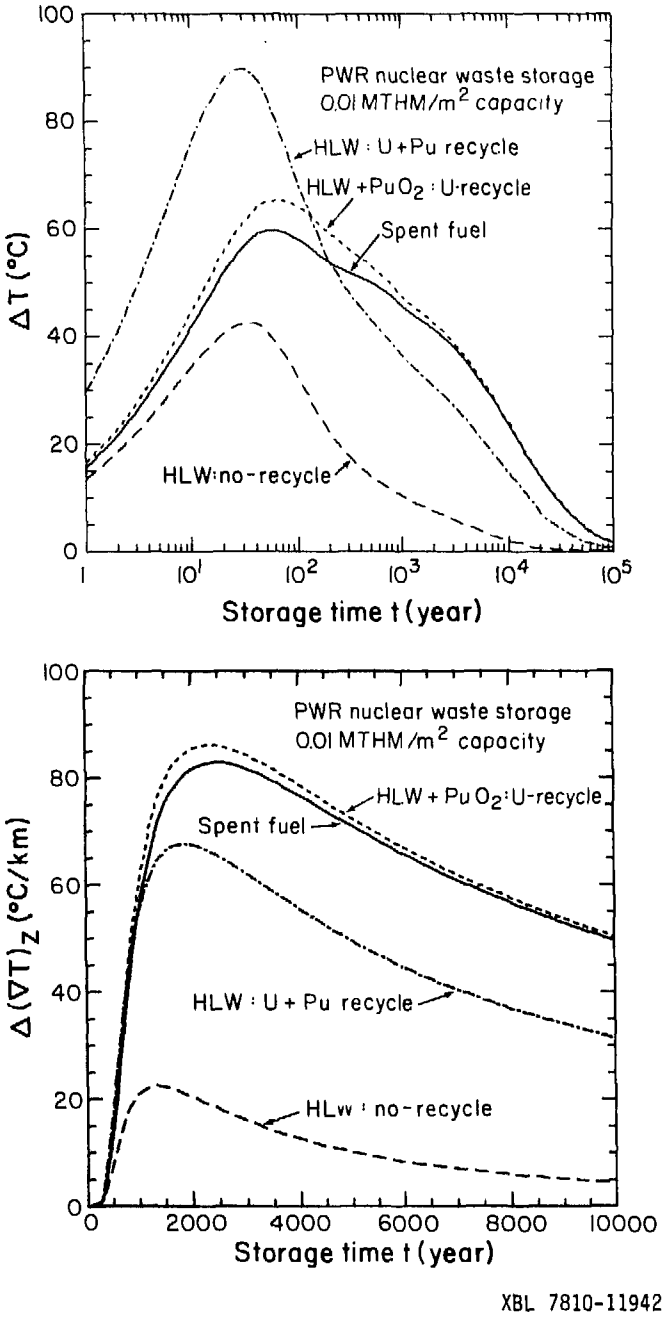

Figure 13. Effects of different PWR fuel cycles from the same amount of fuel on the repository temperature and ground surface thermal gradient.

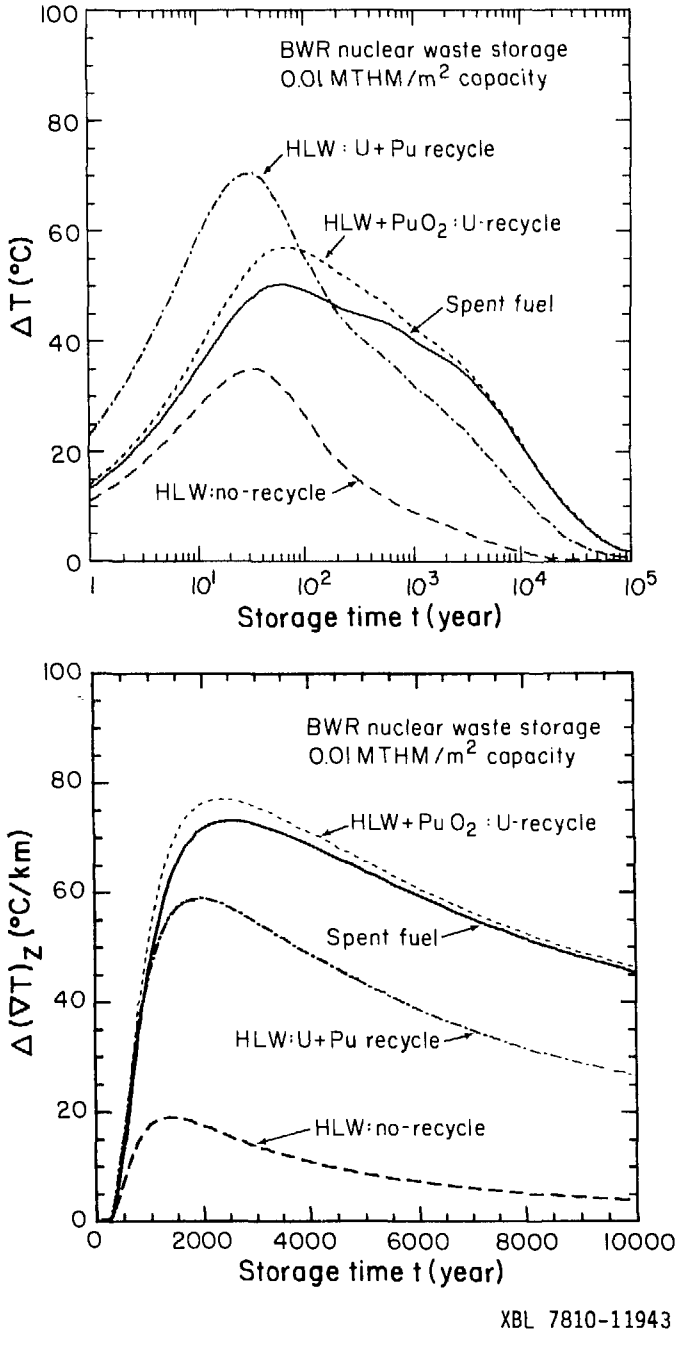

Figure 14. Effects of different BWR fuel cycles from the same amount of fuel on the repository temperature and ground surface thermal gradient.

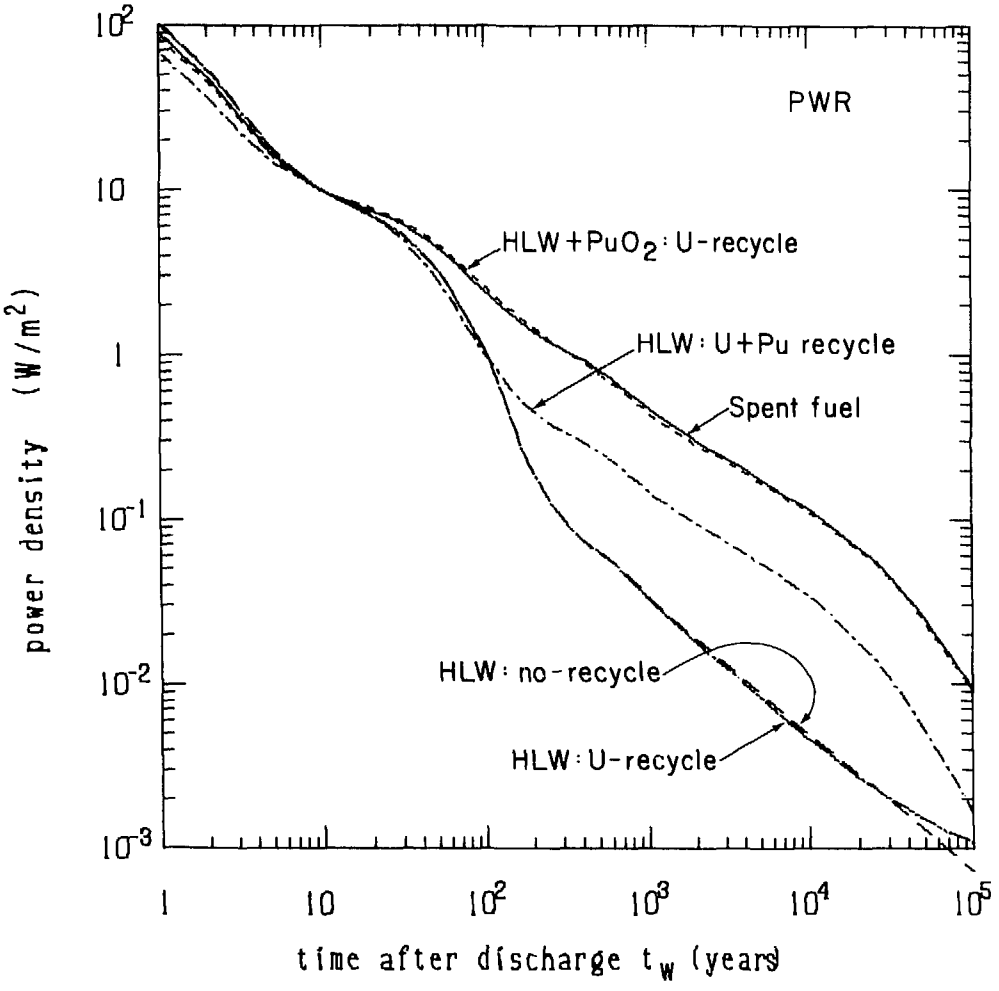

Figure 15. Areal power densities of wastes from different PWR fuel cycles normalized to 10 W/m^2 at 10 years after discharge from the reactor.

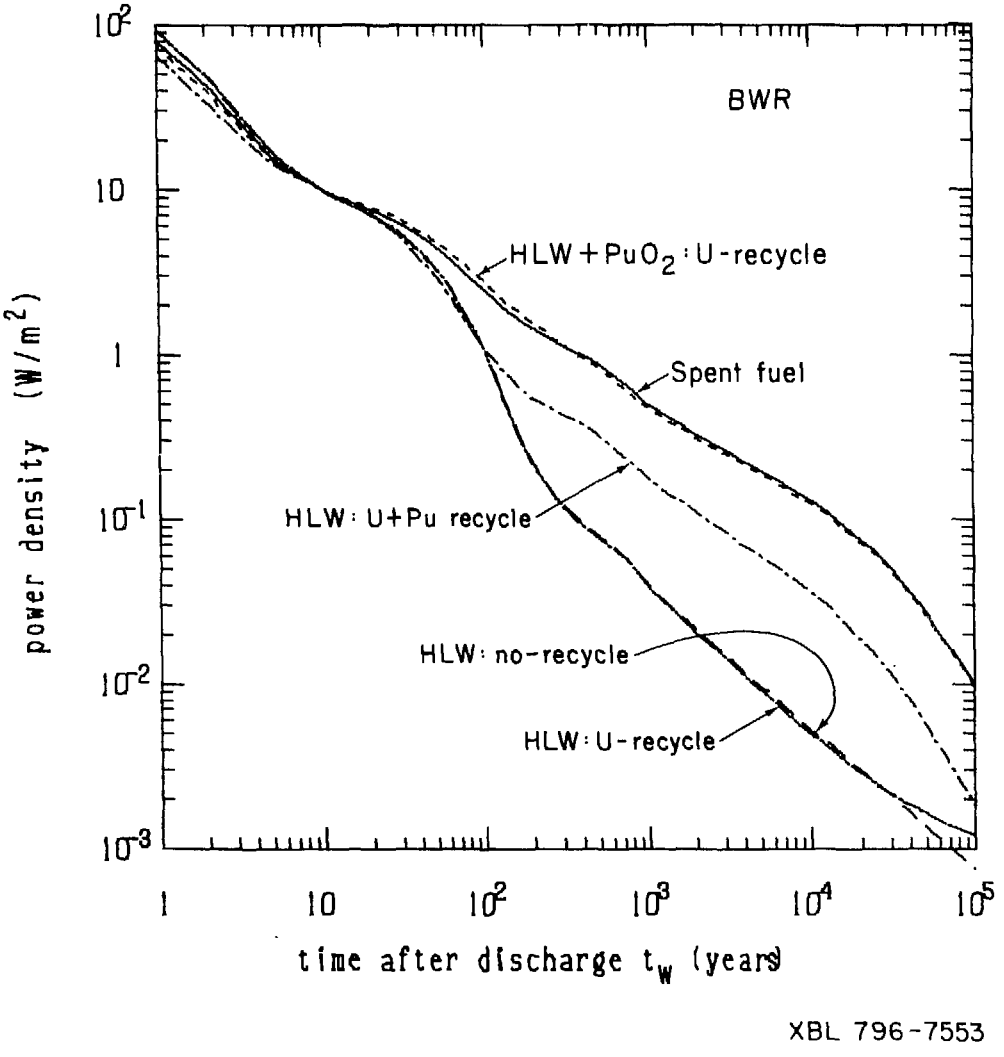

Figure 16. Areal power densities of wastes from different BWR fuel cycles normalized to 10 W/m^2 at 10 years after discharge from the reactor.

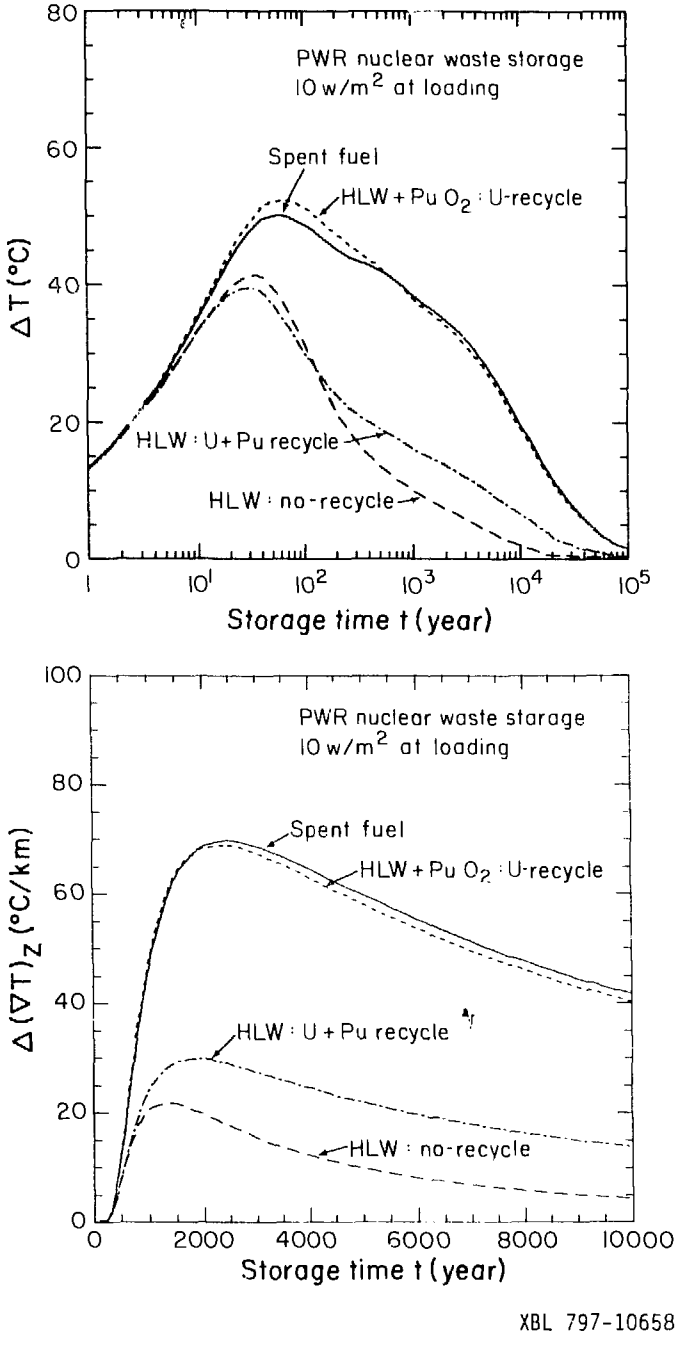

Figure 17. Effects of different PWR fuel cycles with the same initial power density on the repository temperature and ground surface thermal gradient.

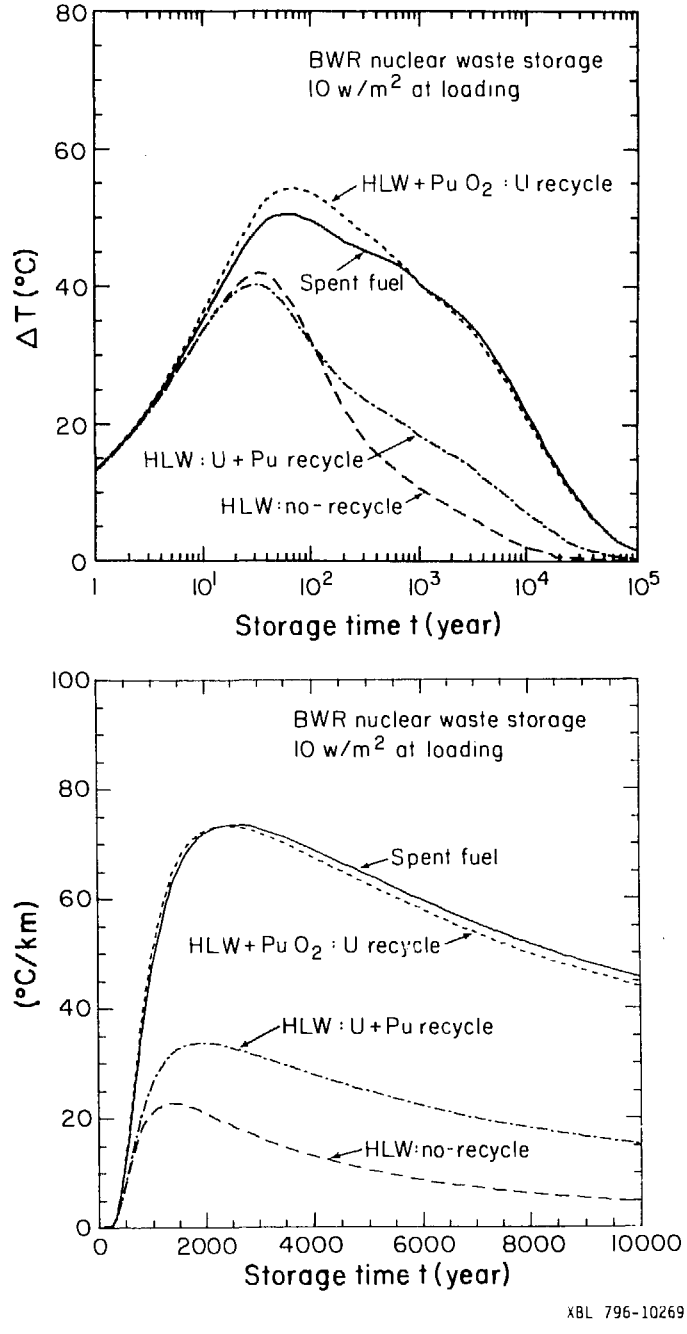

Figure 18. Effects of different BWR fuel cycles with the same initial power density on the repository temperature and ground surface thermal gradient.

Near Surface Cooling Before Emplacement

The power output of all nuclear wastes decays very rapidly immediately after discharge from the reactor. Accordingly, the effects of a period of near-surface cooling of these wastes before burial in a repository may be expected to be significant. The effects over short periods of near-surface cooling on spent fuel and reprocessed waste for PWR (with initial loading densities of 0.01 MTHM/m^2 and 10 W/m^2) on the maximum repository temperatures and epicentral thermal gradients have been calculated and are given in Table 4. The effects of the period of near-surface cooling on the maximum repository temperatures and epicentral thermal gradients as a function of time are also illustrated in Figures 19 and 20. With the early rapid changes of the power of wastes, the results for 0.01 MTHM/m^2 and 10 W/m^2 are very different. From these data, it must be concluded that the period for which the wastes are cooled near surface before burial is an important factor in determining the effect of a repository on the temperatures in the rock mass within which it is located.

Repository Depth and Radius

The effects of different repository depths and radii have been analyzed for situations where the ratio of depth to radius is less than 1. The results are as illustrated in Figures 21 and 22. The maximum temperature is not likely to be affected by this range of depths and radii, but changes in far-field, long-term temperatures must be expected. In particular, the epicentral thermal gradient changes with the ratio of the depth of repository below surface to its radius as illustrated in Figures 21 and 22.

Table 4: Effects of Surface Cooling

Waste form	Surface cooling period	$(\Delta T)_{max}$ [a] °C [c]	$(\Delta(VT)_z)_{max}$ [b] °C/km [c]	Power density at loading W/m^2 [c]	kW/canister
Spent fuel of PWR	1 year	98 (9)	93 (9)	104. (10)	4.81
	2 years	76 (14)	90 (16)	56.4 (10)	2.60
	5 years	67 (33)	86 (43)	20.1 (10)	.927
	10 years	60 (50)	83 (70)	11.9 (10)	.548
Reprocessed waste (no recycle) of PWR	1 year	95 (9)	35 (3)	103. (10)	21.5
	2 years	62 (11)	31 (6)	55.0 (10)	11.5
	5 years	50 (27)	26 (14)	18.7 (10)	3.9
	10 years	43 (41)	22 (22)	10.3 (10)	2.16

a $(\Delta T)_{max}$: maximum value of the average temperature rise at the center of the repository.

b $(\Delta(VT)_z)_{max}$: maximum value of the ground surface thermal gradient rise at the epicenter above the repository.

c Values without parentheses correspond to 0.01 MTHM/m^2 waste capacity.

Values with parentheses correspond to 10 W/m^2 power density.

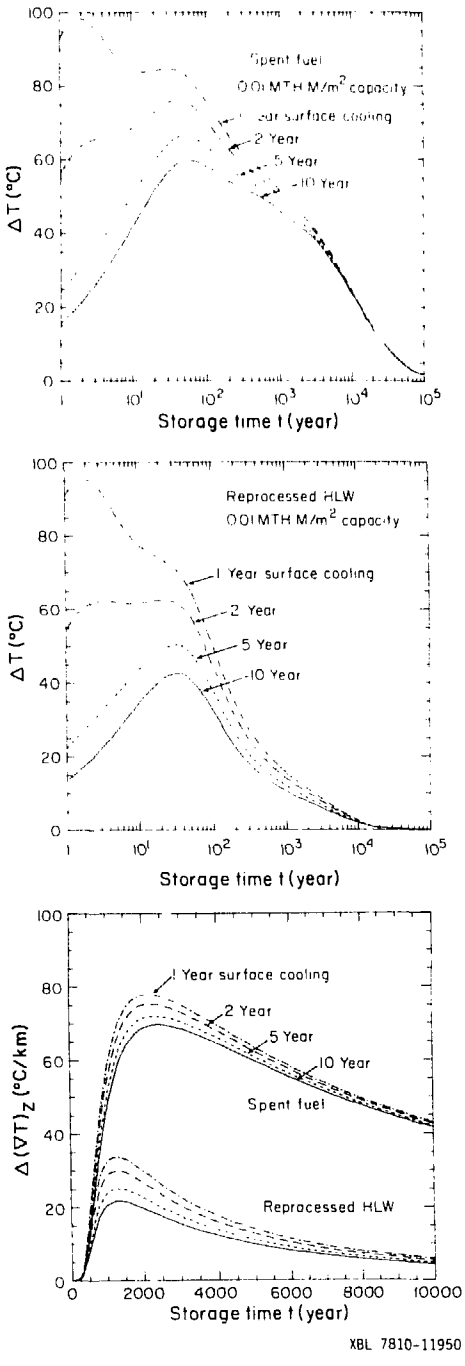

Figure 19. Effects of surface cooling periods of wastes with density of 0.01 MTHM/m^2 on the repository temperature and ground surface thermal gradient.

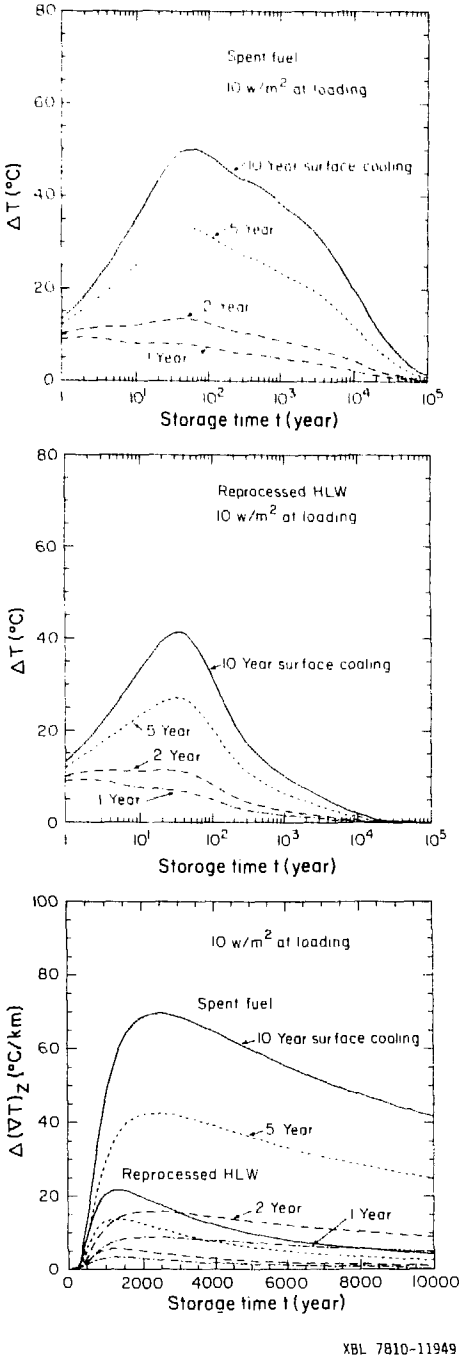

Figure 20. Effects of surface cooling periods of wastes with initial power density of 10 W/m^2 on the repository temperature and ground surface thermal gradient.

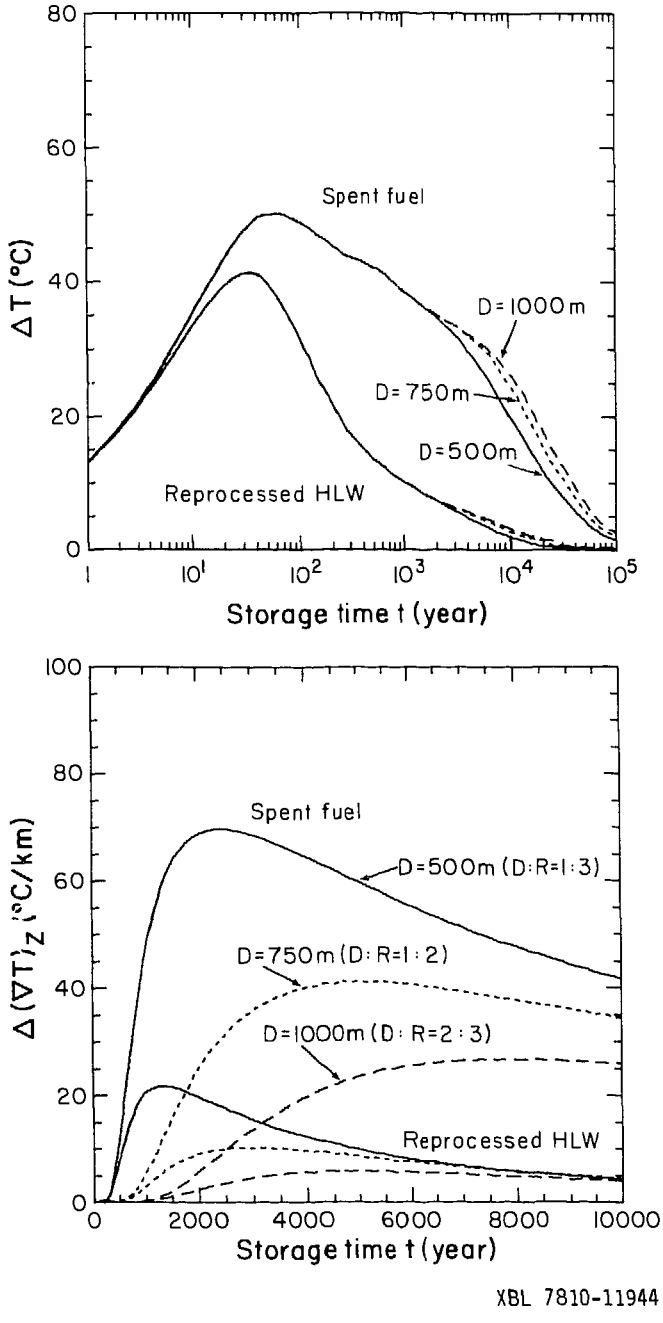

Figure 21. Effects of depths of repository on the repository temperature and ground surface thermal gradient.

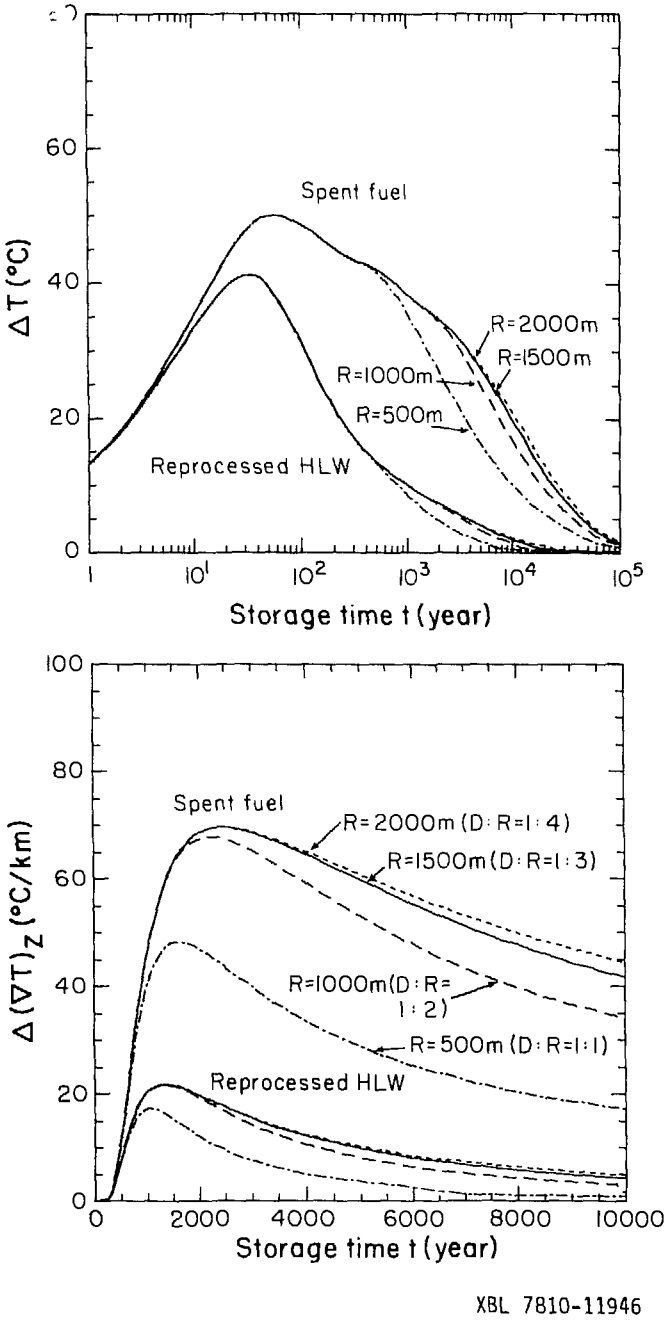

Figure 22. Effects of radii of repository on the repository temperature and ground surface thermal gradient.

Rock Properties

The properties of typical hard rocks were given in Table 1. Using these values the maximum repository temperature and the epicentral thermal gradient have been calculated for a repository loaded with spent fuel or reprocessed waste and the results are as illustrated in Figure 23. From this figure, it can be seen that significant changes in these parameters result from the different rock properties.

The maximum repository temperature can be approximated by

$$\Delta T(0, 0, t_{max}) \simeq \frac{0.3\psi(0)\sqrt{\kappa_T t_{max}}}{K}$$

with t_{max} = 57 years for spent fuel and t_{max} = 37 years for reprocessed waste. The value of $\sqrt{\kappa_T}/K$ for granite and basalt are almost equal to each other. The temperature rises at a repository in granite and in basalt are almost the same at early time and are about six-tenths the value in shale. On the ground surface, the time for the epicentral thermal gradient to reach maximum is approximately proportional to $1/\kappa_T$. The heat diffusion in granite with large diffusivity will reach the ground surface earlier than in basalt and in shale. The maximum value of epicentral thermal gradient is approximately proportional to $\kappa_T^{2/3}/K$ for spent fuel and to κ_T/K for reprocessed waste.

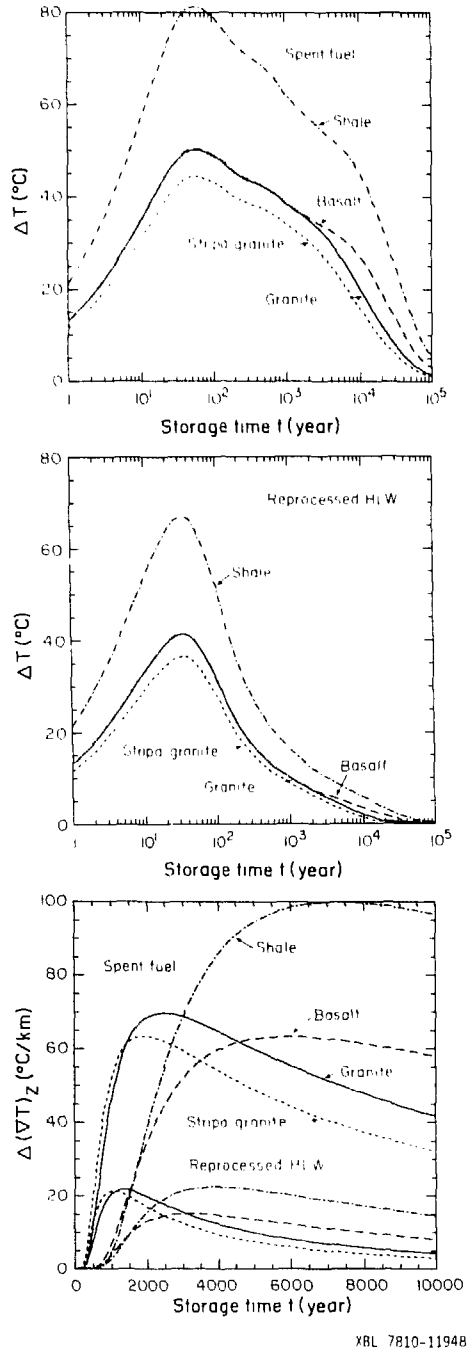

Figure 23. Effects of rock formations on the repository temperature and ground surface thermal gradient.

THERMOHYDROLOGICAL EFFECTS

Fracture Flow Model

Changes in the temperature of the rock mass containing a repository will change the temprature of the groundwater in this rock mass. Increasing the groundwater temperature results in decreased density and viscosity of the water. In this section changes in buoyant groundwater flow induced by these temperature changes are evaluated.

The model used for this purpose comprises a simple horizontal fracture at the depth of the repository connecting a recharge zone to a discharge zone and intersecting a vertical fracture containing the axis of the repository as is illustrated in Figure 24. Flow from the repository to the surface occurs through the vertical fracture. If the effective hydraulic aperture of the horizontal fracture is b_x the permeability $k_x = b_x^2/12$ for laminar fracture flow (Lamb, 1932; Snow, 1965; Iwai, 1977) is assumed in the calculation. Similarly, the aperture and permeability of the vertical fracture are b_z and $k_z = b_z^2/12$, respectively. The flow of groundwater is confined within these fractures. In practice the flow of groundwater through most hard rock, which generally has very low intrinsic permeability (Brace et al., 1968), is largely through fractures. Thus, this model approximates the mechanics of groundwater flow through hard rock masses, differing only in its simplicity.

Before the repository is loaded and the rock mass subjected to changes in temperature, it is assumed that the original groundwater flow is horizontal

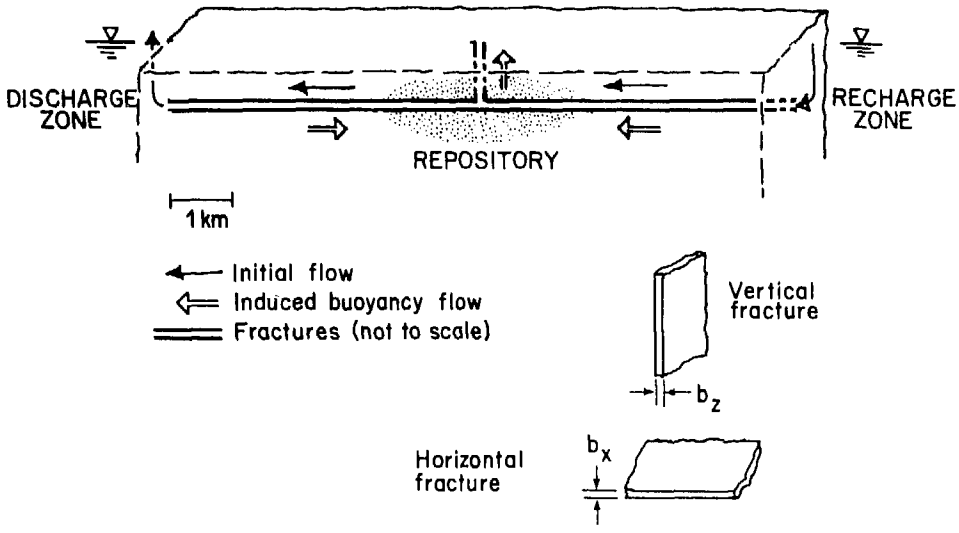

Figure 24. Two-fracture model for simulating buoyant groundwater movement through a repository located between the recharge and discharge zones.

from recharge zone to discharge zone. As the rock mass heats up so will the groundwater in the vertical fracture containing the center of the repository. This will perturb the original flow pattern.

Flow Equations

For any temperature field, the flow of the groundwater must satisfy the equations of conservation of mass and momentum. The equation for the conservation of mass is:

$$\frac{\partial \rho}{\partial t} + \nabla \cdot \vec{q} = 0 \tag{4}$$

where

$\vec{q}$ = the mass flux that is the product of the density and velocity of the water in the fracture;

ρ = density of water; and

t = time.

For low velocities, inertial forces are much less than viscous forces, so that by means of Darcy's law the equation of momentum can be written as:

$$\nabla P + \frac{\nu}{k} \vec{q} + \rho \vec{g} = 0 \tag{5}$$

where

P = pressure;

ν = kinematic viscosity of water;

k = permeability; and

$\vec{g}$ = the gravitational acceleration.

In most studies of thermal convection, because of the small compressibility of water, it is usual to make use of the Boussinesq approximation (Wooding, 1957; Combarnous and Bories, 1975) that variations in the density of water with time can be neglected except for the effects on the buoyancy of the groundwater. As a result of this, equation (4) reduces to:

$$\nabla \cdot \vec{q} = 0. \tag{6}$$

Equations (5) and (6) describe the incompressible flow of groundwater (see Appendix A).

The expression $q_z(t)$ for the simple case with zero regional groundwater flow and the repository located a distance, L, midway between the recharge and discharge zones is considered first. The flow is symmetric about x = 0,

$$P(t) = 0, \qquad \text{at } x = 0,\ z = 0, \tag{7}$$

$$b_x q_x(t) + \frac{1}{2} b_z q_z(t) = 0, \qquad \text{at } x = 0,\ z = -D \tag{8}$$

$$P(t) = P_o = \int_{-D}^{0} \rho_o(z) g dz, \qquad \text{at } x = L,\ z = -D \tag{9}$$

Equation (8) describes Kirchoff's Law for the junction between vertical and horizontal fractures. The hydrostatic pressure at the depth z = -D with a water table at z = 0 is P_o. Before loading the repository and heating of the rock mass, the temperature, $T_o(z)$, as a function of depth, may be given by $T_o(z) = (20 - 0.03z)°C$, where a surface temperature of 20°C and a normal geothermal gradient of 30°C/km is assumed. By imposing a constant pressure boundary condition in equation (9) at the inlet of the horizontal fracture, it is assumed that the temperature at the recharge and discharge zones are not affected by the thermal loading of the repository. This corresponds to

recharge and discharge zones far from the repository or with large heat capacities. The contrast in density between the heated water near the repository and the cooled water in the recharge and discharge zone drives the buoyant groundwater flow in the vertical fracture. The limiting case with zero distance from the repository to the recharge and the discharge zone, L = 0, is an unrealistic representation of the hydrologic condition of a repository (see Appendix B).

In accordance with equation (6), the groundwater flows are independent of the spatial coordinates along the fractures. With constant flow, equation (5) can be integrated from the repository center to the boundary:

$$0 - P(0,-D,t) = -\frac{q_z(t)}{k_z}\int_{-D}^{0} \nu(0,\, z,\, t)dz - \int_{-D}^{0} \nu(0,z,t)g dz, \tag{10}$$

$$P_o - P(0,-D,t) = -\frac{q_x(t)}{k_z}\int_{0}^{L} \nu(x,\, -D,\, t)dx. \tag{11}$$

Equations (8), (10), and (11) can be solved for the unknowns $q_z(t)$, $q_x(t)$ and $P_o(0,-D,t)$. The result for $q_z(t)$ is:

$$q_z(t) = \left[\frac{k_z \rho_o(0) g}{\nu_o(0)}\right]\left[\frac{\Delta h_b(t)}{\bar{D}(t)}\right]\left[\frac{2b_x k_x/\bar{L}(t)}{2b_x k_x/\bar{L}(t) + b_z k/\bar{D}(t)}\right], \tag{12}$$

where

$$\Delta h_b(t) = \int_{-D}^{0} \frac{\rho(0,z,t) - \rho_o(z)}{\rho_o(0)}\, dz; \tag{13}$$

$$\bar{L}(t) = \int_{0}^{L} \frac{\rho(x,-D,t)}{\rho_o(0)}\, dx; \tag{14}$$

$$\bar{D}(t) = \int_{-D}^{0} \frac{\rho(p,z,t)}{\rho_o(0)}\, dz \qquad (15)$$

The factors $\Delta h_b(t)$, L(t), and D(t) have the dimension of length and can be referred to as effective hydraulic heads. Equation (12) is a product of three factors. The first is the hydraulic conductivity of the vertical fracture; the second, the gradient hydraulic conductivity of the vertical fracture (resulting from buoyancy) and the last, a correction for the hydraulic resistance of the horizontal fracture between the recharge and discharge zone and the repository. The product of the last two factors is an effective vertical hydraulic gradient, $(\nabla h)_z$. From equation (12), $q_z(t)$ can be evaluated by the numerical integration of the effective heads, equations (13)-(15). Values for density, $\rho(x,z,t)$ and viscosity $\nu(x,z,t)$ are calculated at the temperature $T_o(z) + \Delta T(x,z,t)$. Values for $\rho_o(z)$ and $\nu_o(z)$ are calculated at $T_o(z)$ (Meyer et al., 1967).

To calculate the displacement of water in the vertical fracture, $q_z(t)$ can be integrated over time. Before loading the repository and heating the rock mass the total amount of static water inside the vertical fracture per unit width is:

$$M_o = b_z \int_{-D}^{0} \rho_o(z)dz. \qquad (16)$$

After heating the rock mass, $q_z(t) = 0$, and the cumulative amount of water flow across a given horizontal section is:

$$M(t) = b_z \int_{0}^{t} q_z(t')dt'. \qquad (17)$$

Water initially at a level $z = -D$ moves upward to a depth given by

$$Z(t) = -D(1 - M(t)/M_o), \tag{18}$$

for $M(t) < M_o$. The vertical displacement $Z(t)$ results from the buoyancy of the water in the vertical fracture.

Equation (12) for $q_z(t)$ can be generalized for the case when $q_o \neq 0$, $L_{rc} \neq L_{dc}$ where the subscripts rc and dc refer, respectively, to recharge and discharge zones. If the original groundwater flow is not zero, the hydraulic heads at the recharge and discharge zones, h_{rc} and h_{dc}, must be different. The pressure difference between the recharge and discharge zones is:

$$VP_o = \int_{h_{dc}}^{h_{rc}} \rho_o(z)\, g dz \simeq \rho_o(0) g(h_{rc} - h_{dc}). \tag{19}$$

From equation (5) the flow in horizontal fracture at the depth $z = -D$ is:

$$q_o = -\frac{k_x \rho_o(0) g}{\nu_o(-D)} (\nabla h)_o$$

where

$$(\nabla h)_o = \frac{h_{rc} - h_{dc}}{L_{rc} + L_{dc}} \tag{20}$$

represents the hydraulic gradient between these zones. The use of the density of water at surface $\rho_o(0)$ and a subsurface viscosity $\nu_o(-D)$ in the equation for the flow q_o is an artifact of this model where water is driven through a horizontal fracture by difference in the near-surface water tables.

To derive $q_z(t)$ for $q_o \neq 0$ and $L_{rc} \neq L_{dc}$, $2b_x q_x$ in equation (8) must be replaced by $b_x(q_{rc}(t) - q_{dc}(t))$. The pressure boundary condition in equation (9) is replaced by two equations with the upper limit of the integral

set as h_{rc} or h_{dc} instead of zero, and Darcy's equation is integrated over both horizontal lengths $x > 0$ and $x < 0$. The expression $q_z(t)$ is:

$$q_z(t) = \left[\frac{b_x k_x k_z \rho_o(0) g}{\nu_o(-D)}\right] \cdot \left[\frac{\Delta h_b(t)(1/\bar{L}_{rc}(t) + 1/\bar{L}_{dc}(t)) + (\nabla h)_o(L_{rc}/\bar{L}_{rc}(t) - L_{dc}/\bar{L}_{dc}(t))}{b_z k_z + b_x k_x \bar{D}(t)(1/\bar{L}_{rc}(t) + 1/\bar{L}_{dc}(t))}\right] \quad (21)$$

Note that equation (21) reduces to Equation (12) for $L_{rc} = L_{dc}$, even when $(\nabla h)_o \neq 0$ or $q_o \neq 0$. That is, the buoyant flow in the vertical fracture is independent of the ambient flow in the horizontal fracture for the symmetric case.

Results of Buoyant Flow

Consider first the case where the vertical and horzontal fractures have the same aperture, $b_z = b_x = 1$ μm, with a repository radius of 1500 m and a length to the recharge and discarge source L = 5000 m. Groundwater initially at the depth of the repository will move upward in a vertical fracture as a function of time after the emplacement of the wastes. The results from two repositories at depths of 500 m and 1000 m are plotted in Figure 25. The buoyancy and the movement of the groundwater is proportional to the change in temperature of the rock mass as can be seen by comparison with Figure 4. The vertical flow in the case of spent fuel is substantially greater than that for reprocessed waste. There is little difference due to the change in depth. Essentially the flow of water as a result of buoyancy depends upon the average temperature of the groundwater throughout the length of the vertical fracture.

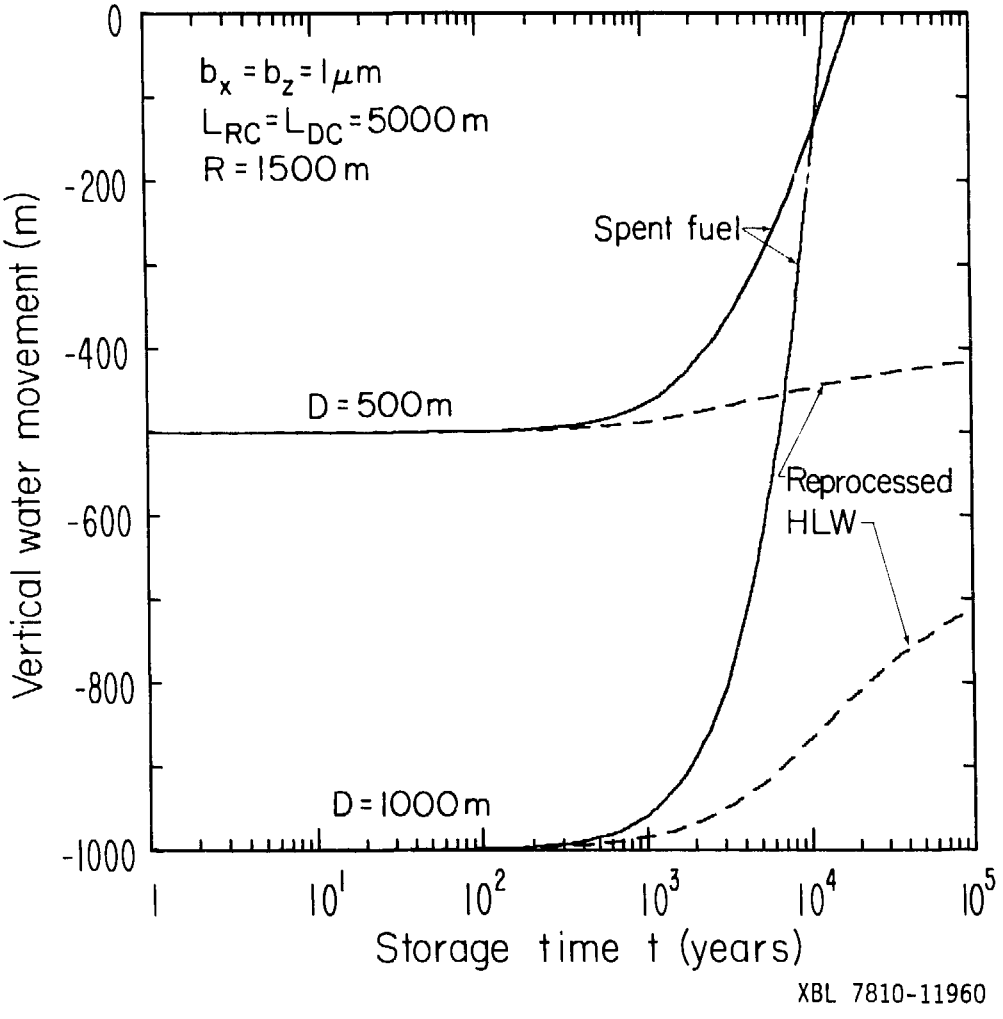

Figure 25. Water movement along vertical fracture from the repository.

In addition to the buoyancy of the heated water in the vertical fracture, the flow of this water is affected by the hydrologic connection between the recharge and discharge zones represented by the horizontal fracture. The shorter the distance from the repository to recharge zone the greater will be the flow of water in the vertical fracture for a given buoyancy. As examples, the velocities have been calculated for distances between the repository and recharge zone at L = 2000 m, 5000 m, 10,000 m and the results are as illustrated in Figures 26 and 27 for repository depths of 500 m and 1000 m. (L = 0 is an unrealistic limiting case, see Appendix B.) The more important factor affecting the buoyant flow of groundwater is the ratio between the distance, L, from repository to the recharge zone and the depth D of the repository.

From equation (12) or equation (21), if the hydraulic resistances of the horizontal fracture were infinite ($b_x = 0$ or $L = \infty$), buoyant flow in the vertical fracture could not occur. For the general realistic case with finite constant values of b_x ($b_x \neq 0$, $b_x \neq B$) and L ($L \neq 0$, $L \neq B$), q(t) does not become infinite as b_z increases. On the contrary, $q_z(t)$ approaches zero as b_z corresponds to ∞; that is, a large vertical fracture with storage capacity reduces buoyant flow. It can be shown that $q_z(t)$ is a maximum value with

$$b_z = \left[\frac{4\bar{D}(t)}{\bar{L}(t)}\right]^{1/3} b_x$$

and

$$q_z(t) \leq \frac{1}{3}\left[\frac{k_x \rho_o(0) g}{\nu_o(0)}\right]\left[\frac{\Delta h_b(t)}{\bar{D}(t)}\right]\left[\frac{4\bar{D}(t)}{\bar{L}(t)}\right]^{2/3} \qquad (22)$$

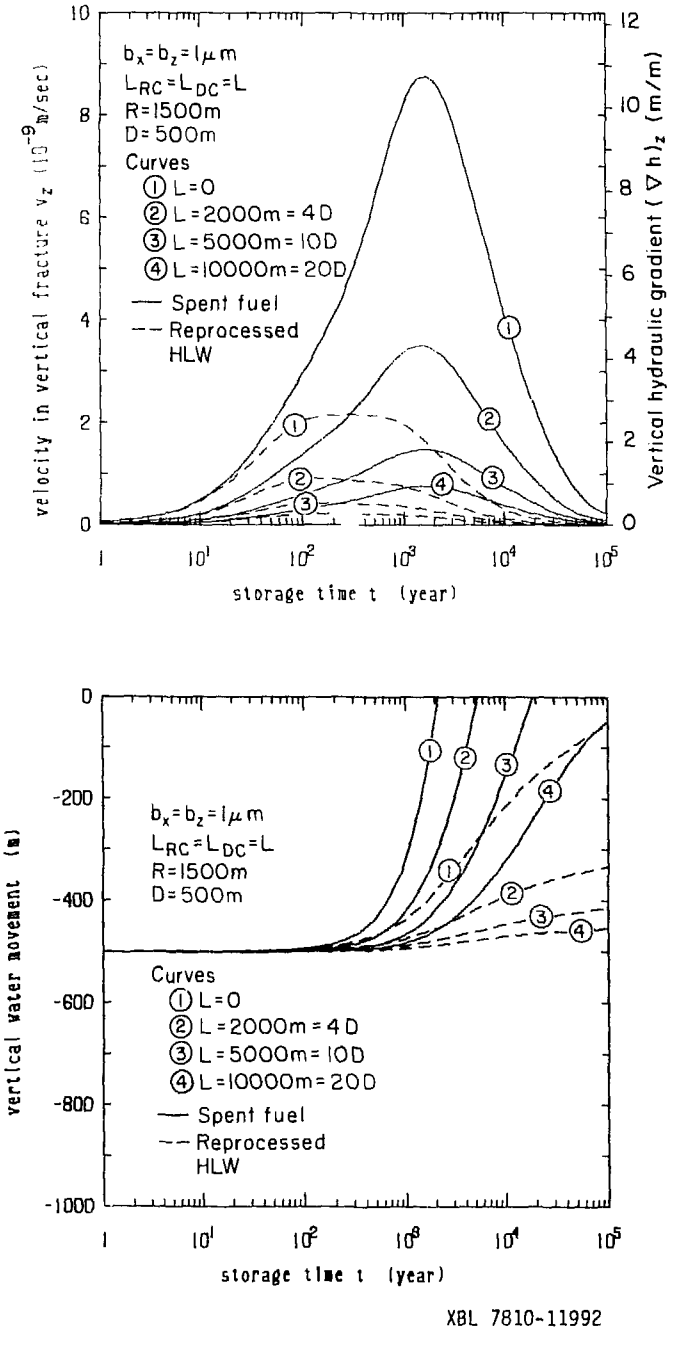

Figure 26. Effects of recharge distances L on the flow velocities, hydraulic gradients, and water movements along the vertical fracture from a 500 m deep repository.

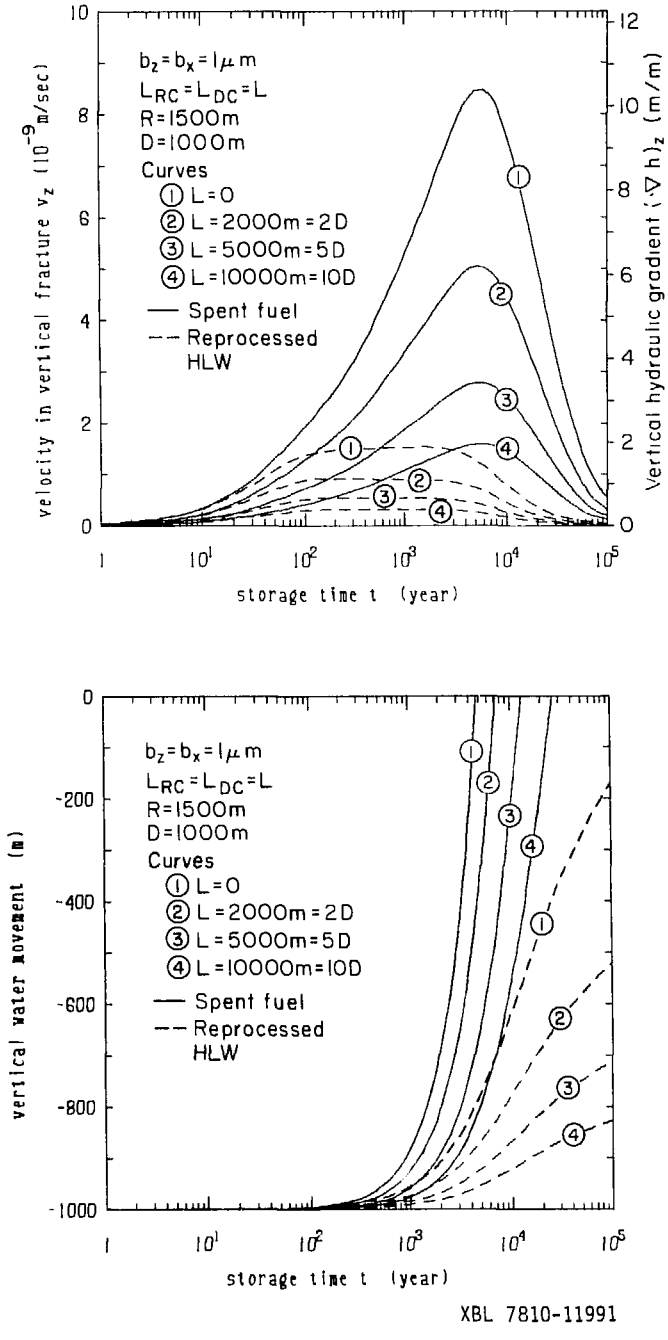

Figure 27. Effects of recharge distances L on the flow velocities, hydraulic gradients, and water movement along the vertical fracture from a 1000 m deep repository.

Buoyant groundwater flow in the vertical fracture has an upper bound which is determined by the permeabilty of the horizontal fracture rather than the permeability of a vertical fracture. In Figure 28 results with a constant aperture b_x = 1 μm and with a range of apertures b_z = 10 μm, 1 μm, and 0.1 μm are illustrated. The movement of the groundwater in the vertical fracture is significantly slower both for the case of $b_z = 10b_x$ and $b_z = 0.1b_x$ than with $b_z = b_x$. The finite recharge capacity through the horizontal fracture restricts the vertical buoyant flow.

All the preceding results have been calculated for the symmetrical situation. In Figure 29 the effects on the buoyant flow of groundwater in the vertical fracture of the position of the repository between the recharge and discharge zones are illustrated. The vertical buoyant flow is only weakly coupled to the horizontal ambient regional flow from water table differences. Finally, the effect of different original geothermal gradients on buoyant groundwater flow in the vertical fracture has been analyzed as shown in Figure 30 for spent fuel and reprocessed waste. The buoyant flow of groundwater in the vertical fracture decreases slightly as the original geothermal gradient increases.

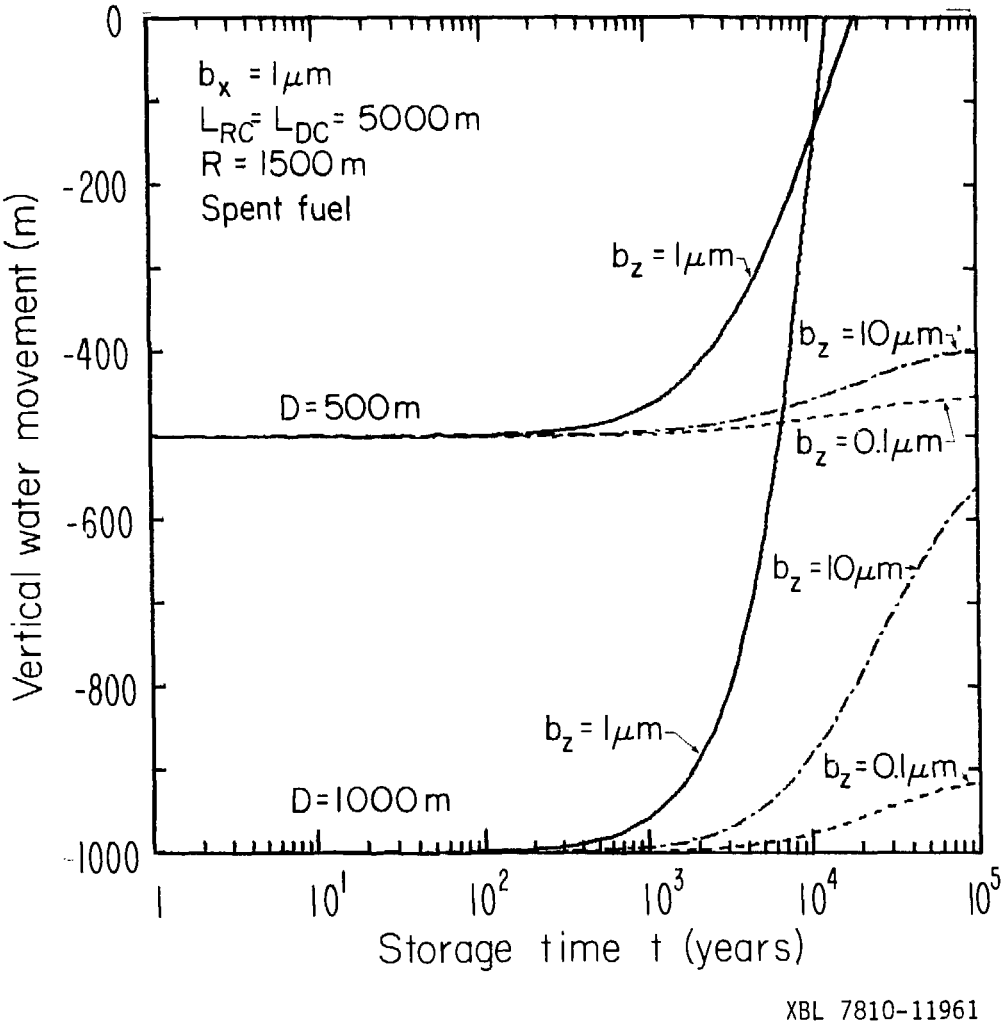

Figure 28. Effects of different vertical fracture apertures on the water movement along the vertical fracture from the repository.

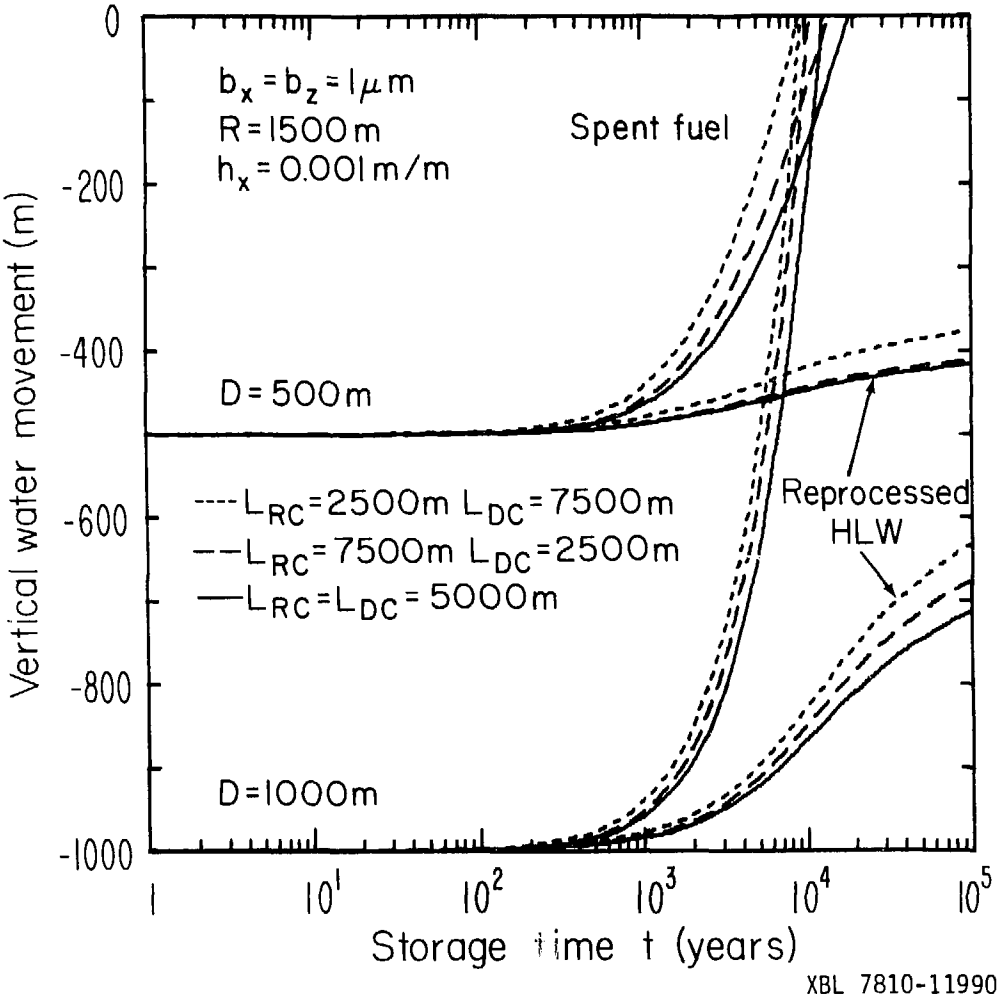

Figure 29. Effects of different recharge distance L_{rc} and discharge distance L_{dc} on the water movement along the vertical fracture from the repository.

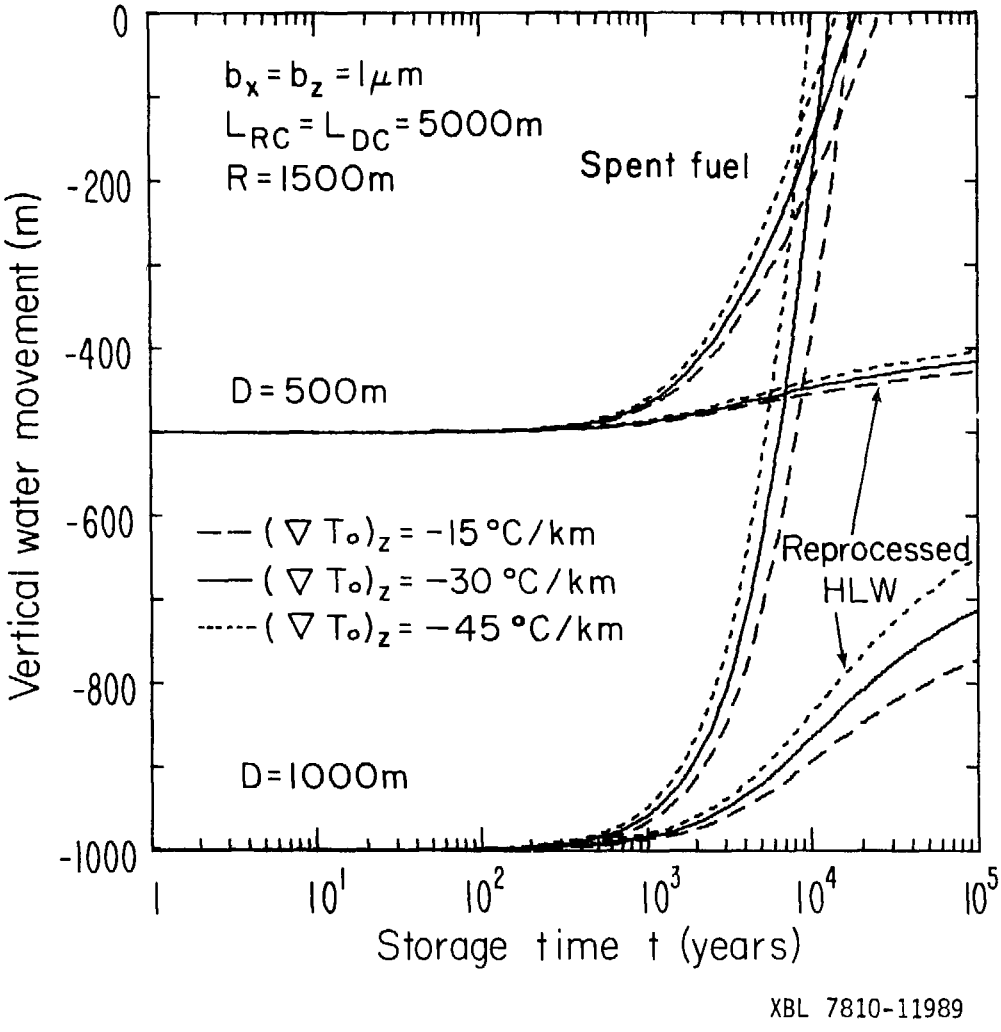

Figure 30. Effects of different original geothermal gradients on the water movement along the vertical fracture from the repository.

DISCUSSION

Although the thermohydrologic model used for the analysis presented in this paper is very simple, it should possess the same physical behavior as that of the more complex systems of fractures which account for the permeability of masses of hard rock. Accordingly, it should provide a good insight into the dynamics of thermally-induced groundwater flow and illustrate the sensitivity of this flow to various parameters. However, the actual numerical results should be considered as no more than an order of magnitude estimations. It must be pointed out also that the transport of nuclides from the repository to surface does not take place at the same rate as that of the groundwater. Nuclide transport is retarded in a certain degree as results of physical and chemical processes, such as sorption.

The calculations reported in this paper suggest that, under certain circumstances, thermally-induced buoyant groundwater flow may be a mechanism by which toxic materials from a repository could be transported to the biosphere. The magnitude of this flow depends upon many factors. Of these, the aggregate increase in the temperature of the rock mass containing the repository is one of the most important. This temperature is affected by the design of the repository, the kind of nuclear waste buried in it, and the period for which this waste has been cooled near surface before burial. Significant differences exist between reprocessed waste and spent fuel in respect of the degree to which the rock mass is heated and hence the time taken for groundwater to reach the surface by buoyant flow. The depth of the repository below surface

is of much less significance. Cooling of the wastes near surface can be used to compensate for these differences and reduce substantially the total amount of heat put into the rock mass. The heat capacity of different kinds of rocks has a significant effect on buoyant groundwater flow also. Finally, the buoyant groundwater flow depends upon the ratio of the hydraulic transmissivities of the vertical and horizontal fractures, the maximum flow being determined by the transmissivity of the horizontal fracture.

REFERENCES

Brace, W. F., J. B. Walsh, and W. T. Frangos. Permeability of granite under high pressure: J. Geophys. Res., 73 (6), pp. 2225-2236, 1968.

Carslaw, H. S. and J. C. Jaeger. Conduction of heat in solids; Oxford at the Clarendon Press, 2nd ed., p. 260, 1959.

Combarnous, M. A. and S. A. Bories. Hydrothermal convection in saturated porous media. Adv. in Hydroscience, 10 , pp. 231-307, edited by V. T. Chow, Academic Press, Inc., New York, 1975.

Department of Energy, Report of task force for review of nuclear waste management, DOE/ER-0004/D, UC-70, Washington, D.C., U.S. Department of Energy, Directorate of Energy Research, February 1978.

Fairchild, P. D., G. D. Brunton and J. F. Cuderman. National waste terminal storage program on radioactive waste storage; Program progress report. Y/OWI-8, Office of Waste Isolation, Oak Ridge National Laboratory, Oak Ridge, Tennessee, p. 133, November 1976.

Hodgkinson, D. P. and P. J. Bourke. The far field heating effects of a radioactive waste depository in hard rock. Seminar on in situ heating experiments in geological formations, Stripa, Sweden, September 1978.

Hood, M. Some results from a field investigation of thermomechanical loading of a rock mass when heater canisters are emplaced in the rock. Presented at the 20th U.S. Symposium on Rock Mechanics, Austin, Texas, June 4-6, 1979.

Interagency Review Group on Nuclear Waste Management. Subground report on alternative technology strategies for the isolation of nuclear waste. TID-28818, October 1978.

Iwai, K. Fundamental studies of fluid flow through a simple fracture. Ph.D. Thesis, University of California, Berkeley, 1977.

Kappelmeyer, O. and R. Haenel. Geothermics with special reference to application. Geopublication Associates, Berlin, Stuttgart, 1974.

Kisner, R. A., J. R. Marshall, D. W. Turner, and J. E. Vath. Nuclear waste projections and source-term data for FY 1977. Y/OWI/TM-34, Office of Waste Isolation, Oak Ridge National Laboratory, Oak Ridge, Tennessee, April 1978.

Lamb, H. Hydrodynamics. Cambridge University Press, New York, 6th Edition, p. 584, 1932.

Maini, T. and G. Hocking. An examination of the feasibility of hydrologic isolation of high level waste repository in crystalline rock. Invited paper, annual meeting of the Geological Society of America, Seattle, Washington, 1977.

Martinez-Baez, L. F. and C. H. Amick. Thermal properties of Cable Mountain basalt cores. Hanford Nuclear Reservation, LBL-7038, Lawrence Berkeley Laboratory, Berkeley, California, 1978.

Meyer, C. A., R. B. McClintock, G. J. Silvestri, and R. C. Spencer, Jr. 1967 ASME steam tables. The American Society of Mechanical Engineers, New York, New York, 1967.

National Research Council. The disposal of radioactive waste on land. Committee on Waste Disposal, Division of Earth Sciences, National Academy of Sciences, Washington, D.C., 1957.

Pratt, H. R., T. A. Schrauf, L. A. Bills, and W. A. Hustralid. Thermal and mechanical properties of granite. Stripa, Sweden; TR-77-92, Terra Tek, Salt Lake City, Utah, October 1977.

Snow, D. T. A parallel-plate model of permeable fractured media. Ph.D. Thesis, University of California, Berkeley, California, 1965.

Wang, J. S. Y., T. N. Narasimhan, C. F. Tsang, P. A. Witherspoon. Transient flow in tight fractures. Invitational Well-Testing Symposium Proceedings, LBL-7027, pp. 103-116, Lawrence Berkeley Laboratory, Berkeley, California, 1977.

Wooding, R. A. Steady free thermal convecting of liquid in a saturated permeable medium. J. Fluid Mech. 2, pp 253-285, 1957.

Appendix A

INCOMPRESSIBLE FLOW APPROXIMATION

The Boussinesq approximation of neglecting the time derivative in the continuity equation

$$\frac{\partial \rho}{\partial t} + \nabla \cdot \vec{q} = 0 \tag{4}$$

and approximating it by

$$\nabla \cdot \vec{q} = 0 \tag{6}$$

can be justified by the following argument: In the usual pressure transient analysis (e.g., Wang et al., 1977), the continuity equation (4) is combined with Darcy's equation without the gravity term,

$$\vec{q} = -\frac{k}{\nu}\nabla P \tag{A1}$$

to yield

$$\nabla^2 P = \frac{\nu}{k}\frac{\partial \rho}{\partial t} \tag{A2}$$

If one further uses the isothermal equation of state:

$$\rho = \rho_o \exp[\beta(P - P_o)] \tag{A3}$$

or

$$\frac{\partial \rho}{\partial t} = \beta\rho \frac{\partial P}{\partial t} \tag{A4}$$

for slightly compressible water, a diffusion equation for the pressure field is obtained:

$$\nabla^2 P = \frac{1}{\kappa_o}\frac{\partial P}{\partial t} \tag{A5}$$

where κ = pressure diffusivity $k/\beta\mu$ and μ = dynamic viscosity $\rho\nu$.

With 1 μm aperture fracture permeability, $k = (10^{-6})^2/12 = 8.3 \times 10^{-14}$ m^2, and standard values for water properties

$$\kappa_p = \frac{k}{\beta\mu} = \frac{8.3 \times 10^{-14}\ m^2}{(5 \times 10^{-10}\ P_a)(0.01\ \text{poise})} = 0.2\ m^2/\text{sec.} \qquad \text{(A6)}$$

The temperature field by heat conduction is also governed by a diffusion equation:

$$\nabla^2 T = \frac{1}{\kappa_T}\frac{\partial T}{\partial t} \qquad (1)$$

The temperature diffusivity $\kappa_T = K/\rho_R C_R$ is typically of order of 10^{-6} m^2/sec (see Table 1). Thus the pressure diffusivity κ_p is much larger than the temperature diffusivity κ_T.

A rough estimate of the transit time for any perturbation to diffuse over a distance D is:

$$\Delta t = \frac{D^2}{4\kappa} \qquad \text{(A7)}$$

This is shown by comparing the temperature transit time $\Delta t_T = D^2/4\kappa_T = 1700$ years with the time of maximum epicentral thermal gradient from a D = 500 m repository (see Figure 7). Therefore, a pressure perturbation will take only $\Delta t_p = D^2/4\kappa_p = 4$ days to reach the surface and is much shorter than the temperature transit time $\Delta t_T = 1700$ years. As the temperature field slowly changes the density and viscosity of water, the induced pressure perturbation will very quickly equilibrate. We may then assume an instantaneous response of the pressure field to the changes in the temperature field. This is equivalent to the approximation of neglecting the transient response and assuming incompressible flow in the convective calculations.

Appendix B

SINGLE FRACTURE MODELS

The two-fracture model considered in this study consists of one horizontal fracture from the recharge zone, through the repository, to the discharge zone; and one vertical fracture from the repository to the ground surface (Figure 24). An even simpler model would have only the vertical fracture as the flow path from the repository to the surface (Maini and Hocking, 1977). The single-fracture model is the limiting case of the two-fracture model with the recharge distance L = 0.

If L = 0, (or equivalently $b_x = \infty$), the open end of the vertical fracture in the repository would be maintained at the hydrostatic pressure P_o of equation (9). Then the vertical fracture could be supplied instantaneously with the cold water for the buoyant flow. This is not a realistic representation of the hydrologic condition of a repository. A repository will be located in a low-permeability formation with a limited supply of groundwater. The horizontal fracture representing the recharge flow path from the ambient water supply must have nonzero length and finite permeability. The inclusion of the horizontal fracture to represent the recharge flow path from charge zones is essential for the simulation of buoyant through flow.

A physically meaningful single vertical fracture is one with a closed end at the repository. If the horizontal fracture of the two-fracture model is completely closed ($b_x = 0$), $q_z(t) = 0$ in equation (12) or equation (21), no buoyant through-flow considered in this study can be developed. Without

recharge, the only possible way for the hot water to flow upward is by developing circulating convective cells within the fracture plane. With small permeability of the fracture and modest heating effect from the repository, vertical convective contribution will be minimal. Only at early time near the perimeter of the repository will cells occur. After a long time, the regional thermal gradient is of the order of the normal geothermal gradient; fast convective motions are unlikely. These possibilities will be discussed in a future report.